PURDUE
UNIVERSITY

AAE 451

METRO-SCOUT

UAV PROPOSAL

SYSTEMS DEFINITION REVIEW DOCUMENTATION

TEAM 4

Kevin Kwan

Dan Pothala

Mohammed Abdul Rahim

Nicole Risley

Sara Tassan

John Thornton

Sean Woock

Alvin Yip

<u>Table of Contents</u>

EXECUTIVE SUMMARY:

Throughout the world today, there is an increased demand for Unmanned Aerial System (UAS) in many different industries for many different purposes. A particularly high need has developed for UAVs with continuous area coverage capabilities. There are several industries in which these vehicles would be useful; however, few options are available for the customer at an affordable price. In recent years, there has been a realization among aircraft manufacturers and the public in general of the huge potential that exists in a civilian UAS market. Law enforcement and news agencies, with their helicopter fleets, have to deal with acquisition costs in the millions, and operating costs in the thousands of dollars every hour. The market is ready for the introduction of an Unmanned Aerial System that can provide most of the advantages of a helicopter, while providing huge cost savings and eliminating the risks of putting a crew in the air.

The Metro-Scout UAS is being designed specifically around payload packages such as the Cineflex V14 high resolution aerial TV camera, and the ThermaCam SC3000, both of which are recognized as top of the line in their respective categories of news coverage and surveillance. In addition, customers can pick a camera of choice to use as long as it meets weight, size, and mount adaptability requirements for the Metro-Scout. The Metro-Scout will be capable of carrying two similar, but alternate payload load-outs based on the mission requirements. For instance, a customer using the Metro-Scout for news coverage would be able to carry single high-resolution TV camera weighing 67 lbs, while a customer using the Metro-Scout for news coverage would be able to carry a payload package comprised of a low to moderate resolution surveillance day/night/IR camera, a still-shot camera, and a radar gun weighing 64 lbs. The Metro-Scout will be able to take-off from small airports in runway distances as short as 1000 feet. It can travel as far as a 150 miles, and loiter on-station for 5 hours. Current estimates put the gross take-off weight at 600 lbs.

In addition, the Metro-Scout UAS will have competitive acquisition and operation costs, far below the current average for news and law enforcement helicopters, and on par with similar UAVs. Team 4's goal with the Metro-Scout UAS is to provide news coverage and law enforcement customers with a intelligently and collaboratively-designed competitive, efficient UAS to achieve mission objectives with less risk, less expenditure, and a greater degree of customer satisfaction.

1.0 Introduction

1.1 Product Definition

The Metro-Scout will be a remotely flown, multi-purpose Unmanned Aerial System designed to operate over highly populated metropolitan environments safely and quietly, in support of the activities of various news agencies and law enforcement departments nationwide. It will be designed to perform continuous area coverage and meet all current FAA regulations for an Unmanned Aerial System operating in airspace over urban areas in the United States. The aerial activities of news and law enforcement agencies have mission requirements that have distinctly different goals, but similar characteristics in terms of endurance, range, and many other things. Each type of customer would require different payload load-outs for their type of mission. However, both types of mission load-outs have similar payload weights and set-ups, and therefore, a single airframe can satisfy the mission requirements of both types of customers.

2.0 Business Case

2.1 Strategy

Team 4's business strategy is targeted primarily at providing a cost-effective UAS alternative to manned helicopters for many news agencies and law enforcement departments. These agencies have traditionally relied on helicopters for their operations, and incur large expenses in acquisition and operating costs.

To successfully compete, the UAS would need to offer more than just a competitive ability to convince the customer to acquire a new, unproven aerial vehicle and replace or complement the current and proven one.

2.2 Competition

According to market studies conducted by an industry watchdog, (Helicopter International Association), the five year average for 2000-2005 for new turbine helicopter sales to law enforcement agencies has been 40.2 per year making up an average market share of 26.7 % for new turbine helicopter sales. Figures 2.1, 2.2 and 2.3 below chart the trends in the

numbers of helicopter sales to law enforcement and US public service agencies over the previous ten years.
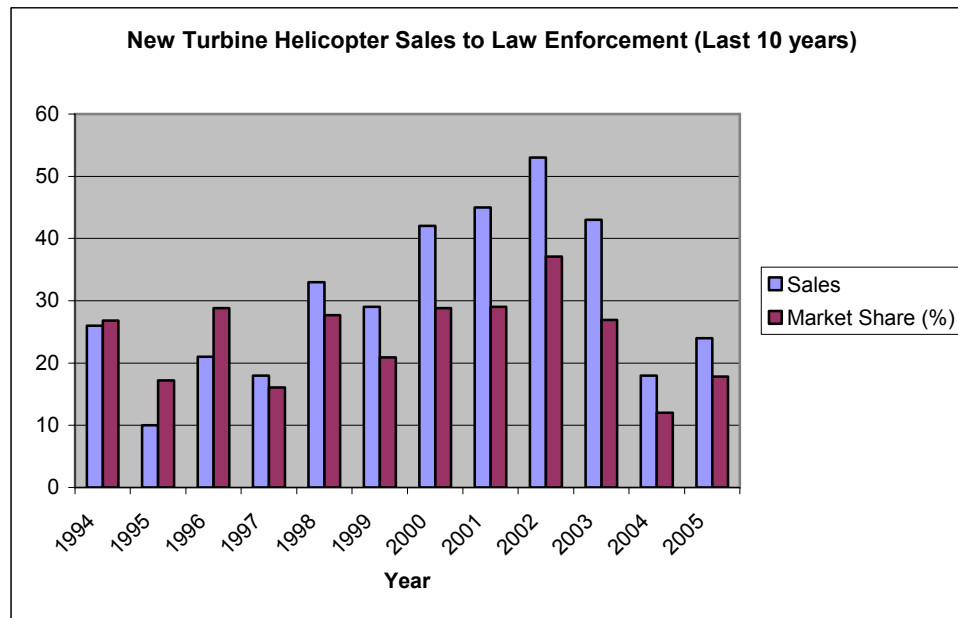
Figure 2.1: 10 year trend for new turbine helicopter sales to law enforcement agencies in the US [1.4]

US PUBLIC SERVICE - TURBINE HELICOPTERS
ANNUAL SALES GROWTH MINUS MILITARY SURPLUS
NET UNIT GROWTH by REGISTERED SALES

September-05

| | NEW | | USED* | | | MILITARY | NET ANNUAL |
	SE	ME	SE	ME	TOTAL	SURPLUS	SALES
2005 YTD	21	3	20	5	49	10	39
2004	16	3	21	*	40	13	27
2003	39	4	17	*	60	5	55
2002	47	6	14	*	67	3	64
2001	41	4	16	*	61	4	57
2000	35	7	19	*	61	12	49
1999	24	5	48	*	77	31	46
1998	29	1	47	*	77	42	35
1997	15	1	132	*	148	126	22
1996	18	0	256	*	274	250	24
1995	9	0	226	*	235	210	25
1994	18	0	80	*	98	65	33
1993	19	5	50	*	74	51	23

* Used SE/ME sales combined in previous years

Figure 2.2: Annual Turbine Helicopter Sales growth to US public service agencies 1993 – 2005

US LAW ENFORCEMENT - PISTON HELICOPTERS
ESTIMATED FLEET

October-05

MODELS	Year End 2004	Additions		2005 YTD Deletions	YTD Change	Current Fleet	Change
		2005 YTD New	2005 YTD Used				
Bell 47 series	32		0	0	0	32	
Enstrom F28	15	0	0	4	-4	11	-26.7%
Hiller UH12	3		0	0	0	3	
Robinson R22	5	0	0	0	0	5	
R44	7	0	0	0	0	7	
Schweizer 269/300C/300CB	97	0	0	1	-1	96	-1.0%
Sikorsky S55	1		0	0	0	1	
Total	160	0	0	5	-5	154	-3.1%

Figure 2.3: Estimated current fleet of piston Helicopters in US law enforcement [1.3]

The two most popular types of rotorcraft in use by news agencies are the Bell 206 Jetranger and the Eurocopter AS-350. Other rotorcraft gaining in popularity are the MD H-500, and Robinson R-44 due to their relative cost-effectiveness. [1.5]

Table 2.1, and figures 2.4 and 2.5 below show the trends for the acquisition and operating costs for various popular competing helicopters in current use.

Aircraft	Acquisition Costs ($)	Hourly Operating Costs ($)
Bell 206B Jetranger	1,200,000	795
Eurocopter AS-350	1,670,000	495
MD H-500 (used 1981)	475,000	211
Robinson R-44	610,000	164
Source: www.aeroads.ca/heliads/search.htm		

Table 2. 1: Competing Helicopter Acquisition and Operating Costs
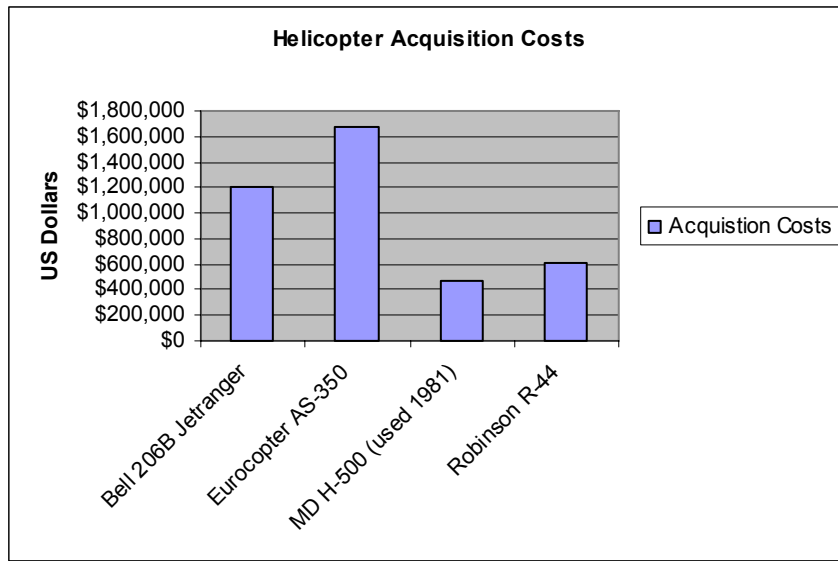
Figure 2.4: Acquisition Costs for various competing helicopters currently in use [6]
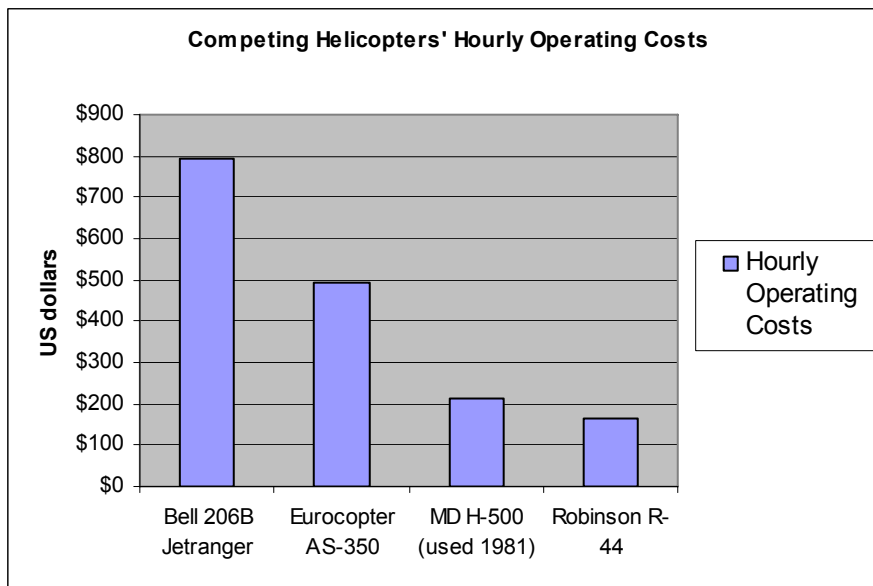
Figure 2.5: Hourly Operating Costs for various competing helicopters currently in use [6]

The Metro-Scout UAS's biggest advantage will be cost. By replacing the helicopter with the Metro-Scout, or supplementing current helicopter operations to lower helicopter flight hours, customers will save in operating and maintenance costs.

Team 4 has set an initial acquisition cost of $350,000 for the Metro-Scout UAS, as this is most competitive price manageable to maintain a decent profit margin, and product quality to compete with helicopters currently used for similar missions. Additionally, Team 4 has established target yearly operating costs for the Metro-Scout UAS of around $10,000 a year.

2.3 Market Size

To estimate the market size, the team researched the existing number of helicopters operating in the United States. According to the Aircraft Owners and Pilots Association (AOPA) of America, there are approximately 7,000 civilian helicopters operating in the US. Of these, about 5,000 are privately owned. This was confirmed by the rotor.com marketplace reports. The rotor.com market letters reported that law enforcement agencies in the US had a total of 154 confirmed active piston helicopters, and 483 confirmed active turbine helicopters in use in the Fall of 2005. These numbers are representative of new helicopters sold to public service agencies in the past 20 years and do not take into account the 797 military surplus turbine helicopters that US public service/law enforcement agencies acquired from the US army between 1993 and 2002. However, the rotor.com reports found that most of these military surplus helicopters have been serving as parts supply for operational helicopters, and Team 4 cannot derive a reasonable estimate for the number of active military surplus helicopters used in law enforcement. The net total for helicopters used by law enforcement today is in the 625-650 range. [1.3], [1.4]

Electronic news eathering is the other target market for the team's product. The two most popular types of rotorcraft in use by news agencies are the Bell 206 Jetranger and the Eurocopter AS-350. Other rotorcraft gaining in popularity are the McDonnell Douglas H-500, and Robinson R-44 due to their relative cost-effectiveness. Team 4 estimated that the total number of active helicopters involved in news gathering was somewhere in the 200-250 range. The team arrived at this estimate by looking at the number of major cities that might require news gathering helicopters. The team estimated conservatively about 100 cities in the US that would have a news market large enough for news helicopters. Also, the team estimated additionally that there are about 40 metropolitan areas in the US large enough to have two or more news agencies with a helicopter on stand-by at all times. [1.5]

From this, the team estimated that law enforcement and news agencies combined were flying nearly 2000 helicopters in the US. This in itself is a sizeable market. However, the relative ease of operability and cost-effectiveness of the Metro-Scout design should make it attractive to a number of smaller News Agencies and law enforcement agencies that cannot afford the cost of owning and operating helicopters. [1.2]

2.4 Market Outlook

Team 4 attempted to develop a realistic prediction of the sales trend for the Metro-Scout Unmanned Aerial System over the course of its expected design life. The team estimated that the Metro-Scout UAS would need a minimum of 3 years for design, testing, and certification. Production is slated to start in the year 2010, with an initial sales estimate of 20 airframes. Team 4 estimated the sales trend from 2010 through 2021 on a classic model describing the introduction of new technology into the industry. Sales are estimated to increase nearly exponentially after the first year, as customers recognize the potential in cost-savings of acquiring the Metro-Scout UAS. The expected sales growth can be attributed to a number of news agencies and law enforcement agencies phasing out portions of their aging helicopter fleets in favor of the UAS. Also, the team expects smaller markets to open up in smaller metropolises in about 5-6 years. At this point, the market for the Metro-Scout model should have realized its full potential. Full-scale production of about a 150 units will only occur around the year 2015, and sales will regress soon after. The reason for the regression is that other manufacturers will catch on to the market potential, and the Metro-Scout will start to become a less competitive option. The team expects this to occur in the 2017-2021 period. However the success of the first model would allow Team 4 to develop a newer more competitive UAS to compete with UASs design by other aircraft manufacturers as they come out. Table 2.2 below lists the expected sales figures in the period 2007-2010 for the Metro-Scout UAS. Figure 2.6 depicts the trend of marketplace technology acceptance, sales growth, realization of full potential, and sales regression expected over the next decade for the Metro-Scout product.

Market Outlook (Expected Sales Figures)					
Year	Metro-Scout Expected Sales	Expected Market Share (%)	Competing Helicopters Sold	Competing UASs sold	Total Market Size
2007	0	0	50	0	50
2008	0	0	50	0	50
2009	0	0	50	0	50
2010	20	30.77	45	0	65
2011	50	50.00	40	10	100
2012	75	53.57	35	30	140
2013	100	58.82	20	50	170
2014	120	63.16	10	60	190
2015	150	64.38	8	75	233
2016	100	48.31	7	100	207
2017	85	41.46	5	115	205
2018	80	38.10	5	125	210
2019	75	36.59	5	125	205
2020	50	27.03	5	130	185
2021	40	21.62	5	140	185
Total Sales	945	533.80	340	960	2245
Yearly Average	63	35.59	22.67	64	149.67

Table 2. 2: Anticipated Market Outlook for the Metro-Scout UAV
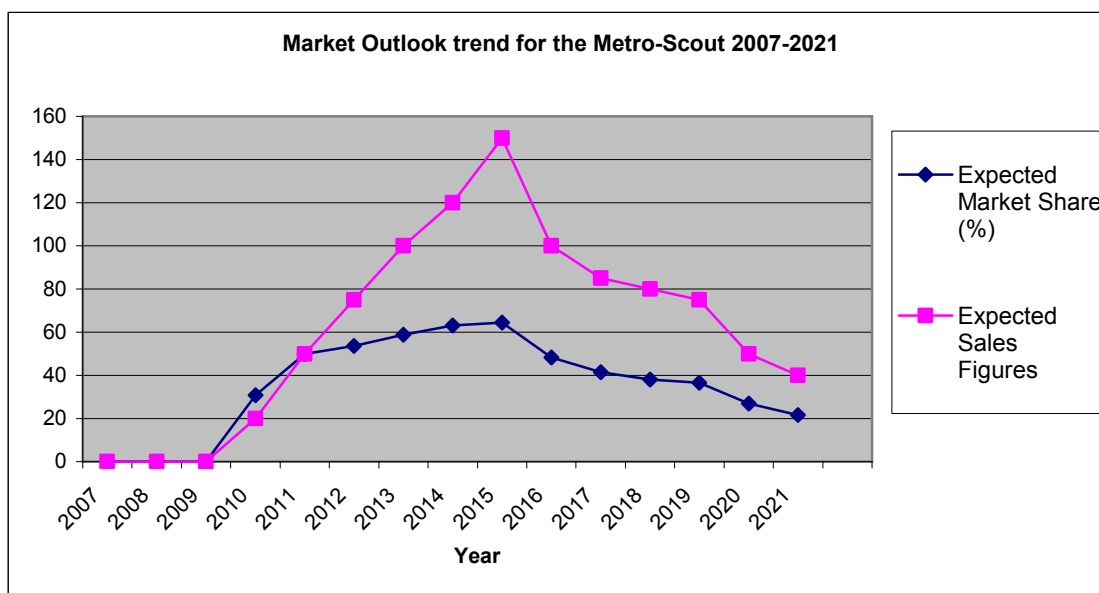
Figure 2.6: Expected market trends for Metro-Scout Sales 2007-2021

As seen from figure 2.6, product acceptance in the marketplace is expected to occur in the period 2009-2011. From thereon, sales growth is expected to occur linearly till the full sales potential is reached around 2015. Sales are expected to then regress as the market receives an influx of newer more competitive UAVs. However, sales are still expected to continue to smaller news agencies and law enforcement agencies due to the Metro-Scout's relative inexpensiveness by the period 2017-2021. Figure 2.7 below highlights Team 4's expected general marketplace trends for the growth of the UAS market among our target customers. It is expected that the size of the UAS market will grow linearly before stabilizing around the year 2025.
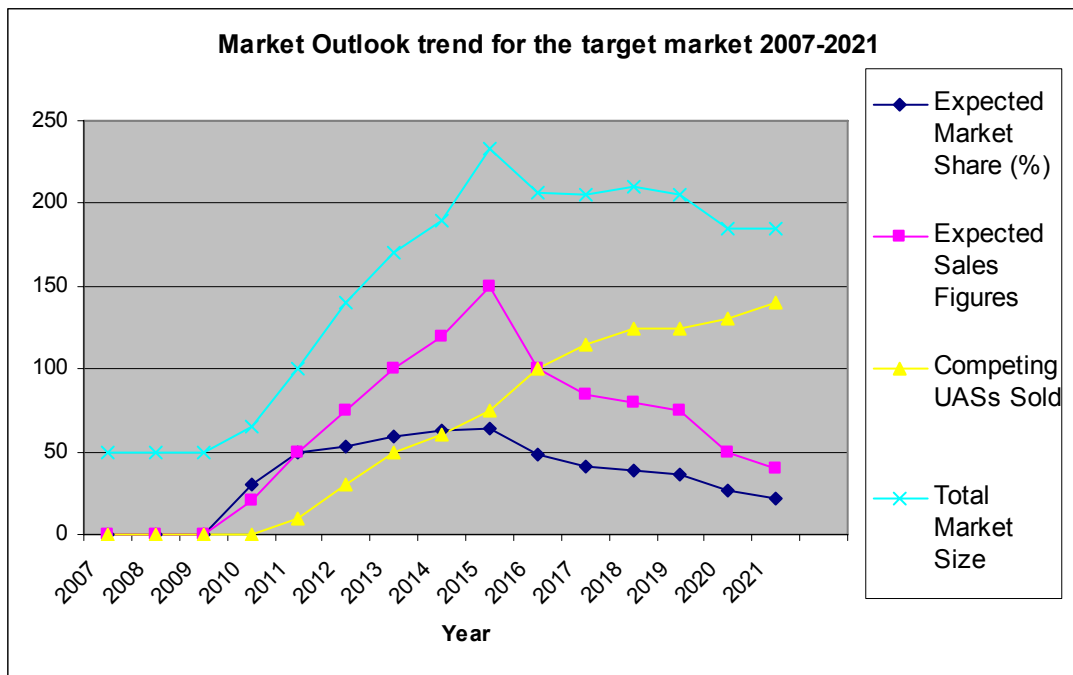
Figure 2.7: Expected Market Trends for UAS sales to Law Enforcement and News Agencies

2.5 Cost Analysis

Team 4 reiterates that these are expected sales figures, and should be considered only potentially representative of the final success of the product. The final step of the team business case was to estimate total monetary returns on the Metro-Scout project. The team formulated an expression for product value depreciation over the years, and incorporated this into the monetary outlook. The team anticipates a net profit of around $105 million at

the end of 2021, from the Metro-Scout program. The details of the monetary return and profits generated on all sales are listed below in Table 2.3.

Year	Metro-Scout Expected Sales	Expected Price Tag ($) with depreciation	Monetary Return ($)	Unit Production Cost ($)	Production Costs ($)
2010	20	350,000.00	7,000,000.00	183500	3,670,000.00
2011	50	350,000.00	17,500,000.00	183500	9,175,000.00
2012	75	340,000.00	25,500,000.00	183500	13,762,500.00
2013	100	330,000.00	33,000,000.00	183500	18,350,000.00
2014	120	315,000.00	37,800,000.00	183500	22,020,000.00
2015	150	300,000.00	45,000,000.00	183,500	27,525,000.00
2016	100	300,000.00	30,000,000.00	183,500	18,350,000.00
2017	85	290,000.00	24,650,000.00	183,500	15,597,500.00
2018	80	290,000.00	23,200,000.00	183,500	14,680,000.00
2019	75	290,000.00	21,750,000.00	183,500	13,762,500.00
2020	50	275,000.00	13,750,000.00	183,500	9,175,000.00
2021	40	275,000.00	11,000,000.00	183,500	7,340,000.00
Totals	945		290,150,000.00		173,407,500.00
Yearly Average	78.75	308,750.00	24,179,166.67	$183,500	14,450,625.00

Table 2. 3: Estimated Monetary Return on Metro-Scout UAS project

Note the price-tag decrease from 2010 through 2021 depicted in Table 2.3. The aircraft itself will sell for an average of $308,750/year if you look at the overall time-span from 2010-2021.

Production and development costs for the Metro-Scout are currently being initially estimated using the DAPCA IV model for lack of a better cost model. The DAPCA IV model was used to estimate:

(1) Program Development (RDT&E) costs: Includes Research, design, analysis, testing, tooling, engineering, and certification.

(2) Production costs: Includes Manufacturing, assembly, materials, quality control, labor, etc.

Table 2.4 below shows the breakdown of costs that go into the Metro-Scout UAS over the 1st five years of production (2010-2015 → 350 airframes approx.).

Program Cost Prediction (*Based on DAPCA IV Model*)				
Classification		*Hours*	*Wrap Rate*	*Cost*
RDT&E:				
	Engineering	85,859	86.00	$7,383,893
	Tooling	46,521	88.00	$4,093,843
	Development Support			$1,254,926
	Flight-Testing			$1,373,039
	Total RDT&E:			$14,105,701
Manufacturing:				
	Manufacturing	395,974	73.00	$28,906,066
	Quality Control	30,094	88.00	$2,648,271
	Mfg. Materials			$7,507,978
	Total Mfg. Cost:			$39,062,315
Flyaway Costs:	Payload Loadout			$50,000
	Avionics			$60,000
	Engine			$10,000
	Approx. Production cost per aircraft:			$183,500

Table 2. 4: Cost Analysis for 1st 5 years using DAPCA IV model

Team 4 estimates a production cost after payload, avionics and engine integration of approximately $183,500 per airframe. Team 4 estimates a market for approximately 950 airframes by 2021 before the Metro-Scout will be retired in favor of newer designs – which would generate sales figures of approximately $120M. Factoring in the development cost of $14.5M, Team 4 estimates a net return on the product of around $105M spread over 11 years. (See Table 2.5 below)

> Net Sales figures   ($ 290,150,000)
> - Production Costs   ($ 170,100,000)
> - Development Costs   ($ 14,500,000)
> =   Net Profit ($ 105,550,000)

Table 2.5: Estimated net return on product

Team 4 estimates approximately **95 airframes** to break even for both production and development costs. The following formula was used to arrive at this figure:

> *Development cost + (n x production cost) = n x Avg. sale price*
>
> (where, n = number of airframes to break even)
>
> ➔ *n = Development Cost / (Avg. Sale price – production cost)*
>
> = $14,500,000 / ($337,000 - $183,500)
>
> = 94.5 … rounded off to 95

Equation 2.1: Developmental Cost

Based on this estimate, the project would break-even by the early second quarter of 2012 (i.e, 2 ½ years into production assuming ideal conditions).

However, if break-even costs were estimated off of the development costs (initial investment) alone, then it would take just **42 airframes** to break even for the initial investment of $14.5 Million.

Figure 2.8 below charts the yearly profit trend and marks out the break-even point for both production and development costs.

Profit vs. Sales by year

Break-Even Point – 95 airframes (1st half, 2012)
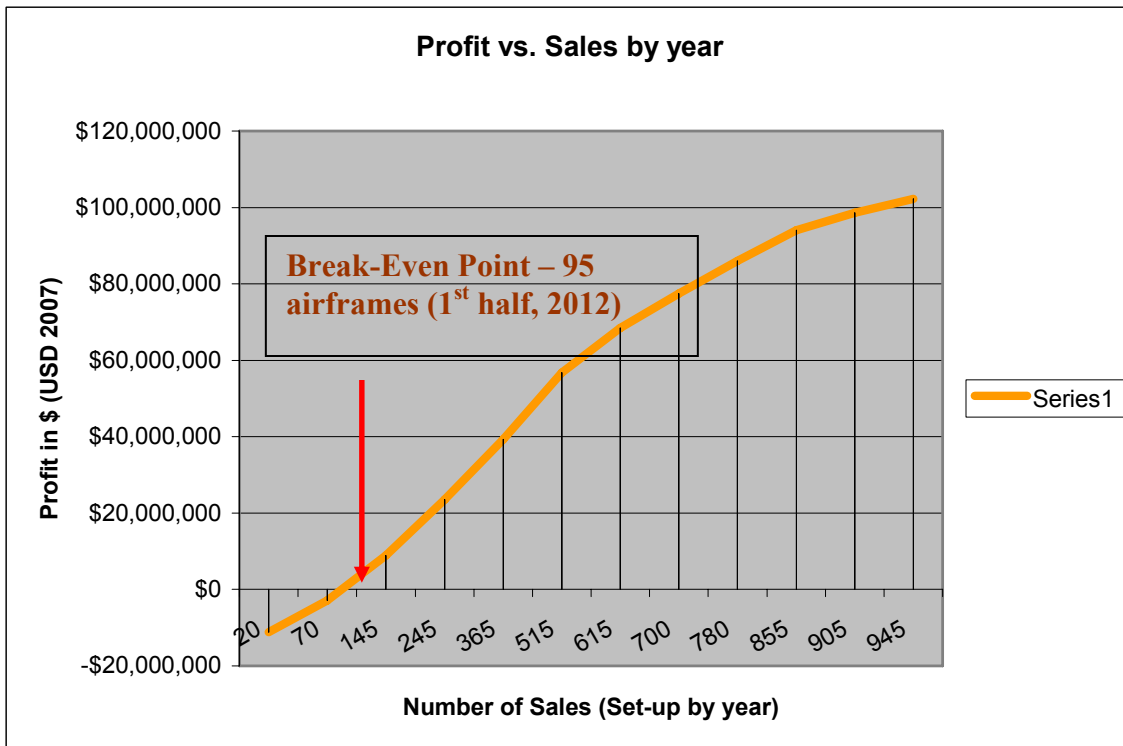
Figure 2.8: Profit trend vs. number of sales highlighting the break-even point for sales

Team 4 will continue to refine its cost analysis for the Metro-Scout, and will attempt to find a more accurate cost model for the Metro-Scout UAS. It is interesting to note, however, that other UAVs within the Metro-Scout's weight and size range have similar acquisition costs – for example, the Shadow UAV produced for the US military by AAI weighs approximately 400 lbs and has a price tag of $275,000 – it also carries more or less the same type of payload, albeit for military operations.

The cost analysis portion of this report is concluded below with a comparison of the costs of the Metro-Scout, and the current best selling helicopter for similar operations – the Bell Jetranger III.

Financial Baseline		
2007 USD	Metro-Scout	Bell Jet-Ranger
Acquisition Cost	$350,000	$1,200,000 + payload price
Operating Expenses	$10,000/year	$20,000/year

3.0 Concept Selection

3.1 Initial Concepts
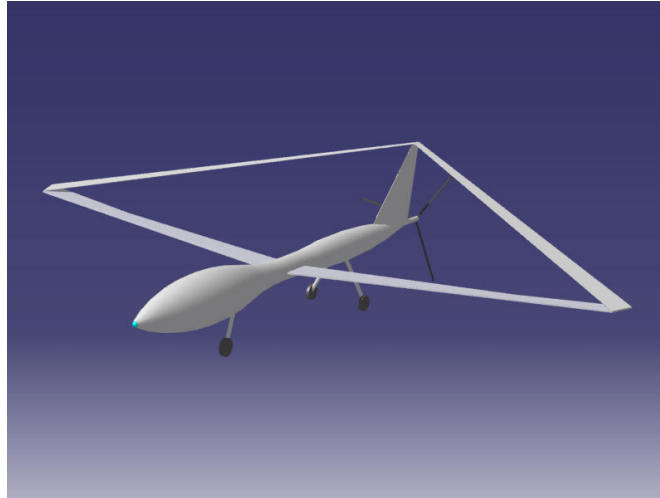
Figure 3.1: Concept I, Box Wing

Concept I, the box wing aircraft, has a front wing swept towards the rear and the rear wing swept towards the front. Unlike regular bi-planes, this arrangement does not include the poor aerodynamic characteristic with vortices from one wing interfering with the other. The main benefit is the significant reduction of structural weight in the order of 30%. The sweep also results in good transonic characteristics. Additional tails are not required as the wings provide enough pitch and roll control. On the other hand this design is difficult to manufacture. The trimmed maximum lift coefficient that's equal to the normal wing-tail configuration is difficult to obtain. There can also be excess wetted wing area and interference drag with many component intersections. [2.1]

Figure 3.2: Concept II, T-Tail

Concept II, the T-tail design, features a pusher propeller on the back of the fuselage with the payload located at the front. A camera pod hangs from beneath the fuselage fore of the nose gear, which is part of a tricycle landing gear configuration. To increase propeller efficiency by keeping the propeller out of the disturbed air from the horizontal stabilizer, this design utilizes a T-tail. This tail configuration places the horizontal stabilizer above the inflow to the propeller. The T-tail configuration also features a smaller wing aspect ratio when compared with other designs.

A disadvantage to the T-tail involves the extra weight incurred in strengthening the vertical stabilizer to support the horizontal stabilizer. This represents a key detriment to the design of an unmanned aerial vehicle for this mission, as the added weight to the very rear of the aircraft (where the engine already resides) shifts the center of gravity quickly aft, decreasing static margin. Such a consideration may null the advantage of reducing the interference of the horizontal stabilizer with inflow to the propeller.
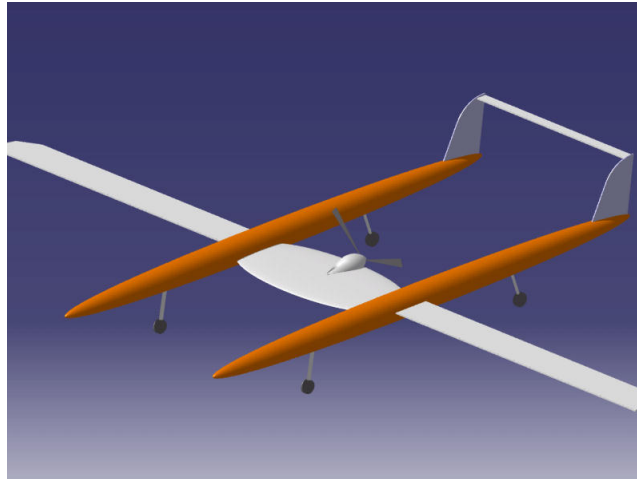
Figure 3.3: Concept III, Twin Fuselage

Concept III, the double fuselage conceptual design, was considered very early on, before the payload had been determined. The idea was that the multiple cameras used in the payload could be spread out between the two fuselages in order to give each a clear line of sight, but still have a balanced weight. Also, there was the possibility of using the extra space to retract the landing gear. Once the two payloads were determined to be a single camera, the purpose of the twin fuselage was voided and gave no advantages over the other designs. In fact, the twin fuselage design showed several disadvantages including its propeller limitations and excess weight.

Figure 3.4: Concept IV, Canard with V-Tail

Concept IV, a V-tail arrangement, was considered. There are some advantages and some disadvantages to using a V-tail. The V-tail, which is lighter in weight than a conventional

tail, contributes to reducing the aircraft's wetted area which in turn reduces skin friction drag. Another advantage is that it provides better ground clearance than a conventional tail; however, the ground clearance would be limited by the pusher propeller engine. The penalty of using V-tail results in control-actuation complexity. Rudder and elevator control inputs must be blended in a mixer to provide the proper movement of the V-tail "ruddervators". In addition, the V-tail causes "adverse roll-yaw coupling" where the ruddervators produce a rolling moment toward the opposite direction/turn that the aircraft is supposed to do. Thus, as stability and control is one of many issues in designing the UAV, the V-tail conceptual design was deemed undesirable.
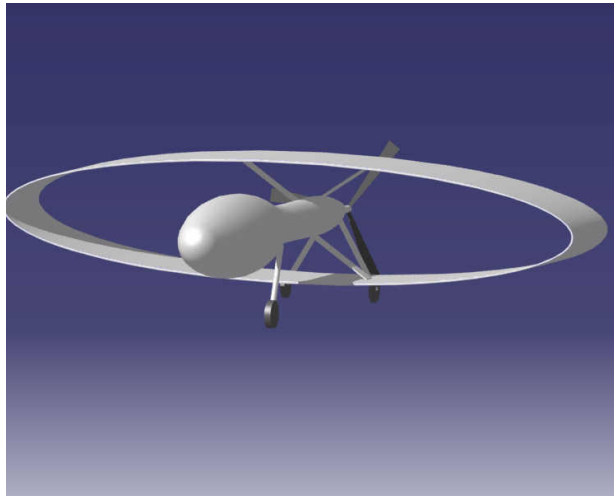
Figure 3.5: Concept V, Ring Wing

Concept V is the most unconventional among the concepts Team 4 selected for review. The ring wing is a derivative of the box-wing and biplane designs with the wing tracing a complete circle/ellipse around the fuselage. Theoretically, a ring-wing design should provide drag benefits, and added lift, in addition to placing all the control surfaces on the wing. The problems with this concept arise from stability, design, and manufacturing complexity required to make it work. These each add to the cost of the overall project.

Figure 3.6: Concept VI, Boom Tail

Concept VI , the boom tail design was designed to maintain stability of the UAV by placing the center of gravity in front of the aerodynamic center. The stability problem associated with a push propeller driven aircraft stem from the engine weight which would move the center of gravity toward the rear end of the aircraft. The wing of the aircraft would need to be placed closer to the rear of the aircraft compared to that of a tracker propeller or tail mounted pusher propeller driven aircraft. Moving the wing back would reduce the moment arm available to the aileron and rudder. A boom tail design overcomes the problem by placing the engine near the center of the aircraft. Center of gravity, in most cases, would fall in front of the aerodynamic center when the payload is placed at the front of the aircraft. The moment arm for the aileron and rudder is thus maintained and the horizontal stabilizer is raised to reduce prop wash and since the propeller is ahead of the tail, there is no interference from the tail to reduce propeller efficiency. The boom tail, however, would increase the weight of the aircraft in order to create a sturdy tail structure.

Figure 3.7: Concept VII, Canard Pusher-prop w/ Vertical Tail

Concept VII depicts a pusher-prop canard aircraft with a single vertical tail, and fixed tricycle landing gear. This is, for the most part, a conventional canard-type aircraft reminiscent of most fighter aircraft designs that incorporate canards, and differing from most of the Burt Rutan designs in terms of not having vertical tails at the wingtips. Also, the main wings have not been swept because the payload weight in the nose provides sufficient ballast to maintain the forward center of gravity within controllable limits so that the engine weight cannot tip the airplane over during rotation for takeoff or landing. This negated the need for wing sweep to move the engine closer to the aircraft center of gravity. The canard configuration also provides desirable stability characteristics. When designed correctly, the canard will stall before the main wing, pushing the nose down and preventing the wing from stalling.

Figure 3.8: Concept VIII, Cruciform

Concept VIII is a conventional aircraft design. It has a vertical tail with horizontal stabilizers. This particular design also incorporates a pusher propeller engine and fixed tricycle landing gear. This is the general design for most general aviation aircraft such as the Cessna 172. There are very few disadvantages to this particular design but as mentioned above there are many more advantages to designs that allow for higher lift. High lift is extremely important for the current mission of the Metro-Scout as it is a small, light aircraft that will loiter for approximately 5 hours.

3.2 Pugh's Method

After conceptualizing several initial design possibilities for the aircraft, the team needed to select the most appropriate concept for the mission. To aid in this selection, the team utilized a tool called Pugh's method of concept selection [3.1]. The goal of this process involves comparing the initial designs generated based on the requirements from the House of Quality developed for system requirement analysis, developing new concepts from the positive aspects of the initial designs, and finally deciding on the best design for the particular mission. A design group rarely selects an initial concept without modification for the final design, as was the case for the team in charge of designing the Metro-Scout.

Pugh's method relies on a matrix of criteria and design concepts as a visual means of comparing aspects of candidate configurations. An example of such a matrix is found in Table 3.1.

			CONCEPTS	
CRITERIA	1	2	3	4
A				
B				
C				
D				

Table 3.1: Pugh's Method Template

The design team initially used criteria directly corresponding to the engineering expectations that comprised the column headings of its QFD House of Quality. This method, however, led to many awkward if not useless comparisons between concepts due to

lack of prior knowledge. For example, one criterion used was L/D (lift-to-drag) ratio.
Comparing designs based on this characteristic proved nearly impossible because the team
had no way of knowing what the final L/D ratio would be for each initial concept. Further
development of the criteria led to ideas that could be easily evaluated with the team's base
knowledge, such as manufacturing cost.

Once the criteria had been selected, the team then selected the original concept it felt best
met the criteria and mission at the time. This became the datum for comparison in the
matrix. Group members then compared each design to the datum based on the selected
criteria using the following notation entered into the corresponding system:

+ : concept meets criterion better than datum

S : concept not clearly better or worse at meeting the criterion than the datum

- : concept meets criterion worse than datum.

Table 3.2 displays the Pugh matrix from table 3.1 after a datum is chosen and compared
with the other concepts.

			CONCEPTS	
CRITERIA	1	2	3	4
A	+	**DATUM**	-	+
B	S	**DATUM**	-	+
C	S	**DATUM**	+	+
D	-	**DATUM**	S	S

Table 3.2: Pugh's Method Example

In table 3.2, concept two (2) represents the datum. The matrix shows that concept one (1) is
more proficient at meeting criteria A than concept two, but not as proficient at meeting
criteria D. This matrix seems to indicate that concept four (4) possesses several advantages
over the datum and, in effect, might complete the mission more effectively. Pugh's method
of selection, however, urges a designer to determine which *features* of a design are most
effective, not necessarily the entire design. The team also added the criteria of design life,

manufacturing cost, and operating cost, considerations that were not present in the House of Quality.

Based on the first iteration of the Pugh matrix, the team developed several new concepts by eliminating adverse aspects and adding advantageous features to the first designs. They then ran the matrix with these new concepts and a new datum. The finished product represented the result of three iterations of the matrix, each with new concepts and new datum designs that produced a synthesis of concepts that best satisfied all criteria.

Section 3.1 describes the initial design concepts drawn by each team member. After developing the proper criteria, the team conducted three iterations of the Pugh matrix using the initial concepts for comparison. Table 3.3 displays the results of the first iteration of the method. For this initial comparison the team selected the boom tail design as the datum considering its lack of interference with pusher propeller inflow while allowing room for substantial horizontal and vertical stabilizer surfaces.

Team members compared each design to the datum in terms of every criterion. As an example of the comparison process, group members considered each design in terms of the criteria of lift and drag (rows ten and eleven in table 3.3). As a matter of reference, designers aimed to minimize drag and maximize lift. Row ten shows that, aside from the T-tail design, no design met the criterion of minimum drag to any greater or lesser extent than the datum boom tail design.

The team surmised that the T-tail might create a large amount of drag at moderate to high angles of attack where the horizontal stabilizer would be placed directly in the turbulent outflow from the propeller. Hence, this design warranted a "-" evaluation in this category. In terms of lift, the Metro-Scout team felt that the box wing design would produce more lift than the boom tail, which involved a standard wing. This decision hinged on the knowledge that well-designed box wings create more lift than standard wing designs. This is the key advantage to a box wing, hence it earns a "+" evaluation when compared to the datum. The T-tail received a "-" in the lift category also. This is due to its lower aspect ratio than the

boom tail design. No other design qualified for an advantage or disadvantage in the category of lift.

		CONCEPTS				
Iteration :		**1**				
		1	2	3	4	5
DATUM HILIGHTED IN RED		Box	Standard	BOOM Tail	T-tail	Canard
CRITERIA						
1	Gross Weight	-	+	\	-	+
2	Fuel-Efficiency	S	S	\	-	S
3	Aspect Ratio	-	S	\	S	S
4	Cruise Speed (Range)	S	S	\	-	S
5	Loiter Speed (endurance)	S	S	\	+	S
6	Loading Capacity	-	+	\	-	+
7	Stability	-	-	\	S	-
8	Maximum Speed	+	S	\	-	S
9	Need for Fly-by-Wire	-	S	\	S	-
10	Drag	S	S	\	-	S
11	Lift	+	S	\	-	S
12	Higher Angle Rate of Climb	+	S	\	S	S
13	Maneuverability	S	S	\	-	S
14	Longer Design Life	-	+	\	+	+
15	Manufacturing Cost	-	+	\	-	S
16	Operation Cost	S	S	\	-	S
Total Positives (+)		3	4	0	2	3
Total Negatives (-)		7	1	0	9	2

Table 3.3: First Iteration of Pugh's Method

After the team completed its evaluation of every concept in each of the sixteen design criteria, the team summed the positive and negative evaluation marks for each design. This action did not give each design a score but rather helped the group evaluate what was poor and advantageous for each design. After careful evaluation of each of these aspects, the canard design became the new datum. While concerns about stability of the canard design existed, it compared well to the other ideas in terms of overall weight (row 1), structural loading capacity (row 6), and design life (row 14). It also met all other categories equally as well as the boom tail design.

Using several hybrid concepts as well as some modified original ideas from the first iteration for comparison with the canard design as the datum, the team performed a second and third iteration of the Pugh matrix. Table 3.4 shows the third iteration, which represents the final design selection of the canard configuration. This iteration indicated that no other concept met the design criteria as efficiently as the canard design. The team deemed some

areas where the canard seemed to be lacking (stability, manufacturing cost, operating cost) recoverable through design. For example, the canard design had potential for being quite unstable without careful consideration, but the team decided it could overcome this disadvantage with proper layout and aerodynamic design. Business case and market analysis also indicated that advantages in design could generate enough additional revenue to null the advantages of the other designs in the categories of manufacturing and operational costs.

Iteration :	3			
CONCEPTS				
DATUM HILIGHTED IN RED	Box	Cruciform	BOOM Tail	Canard
CRITERIA				
1 Gross Weight	-	-	-	\
2 Fuel-Efficiency	+	s	-	\
3 Moderate Aspect Ratio	-	s	s	\
4 Higher Cruise Speed (Range)	-	-	-	\
5 Lower Loiter Speed (endurance)	-	s	-	\
6 Loading Capacity	-	s	-	\
7 Stability	+	+	+	\
8 Maximum Speed	-	-	-	\
9 Need for Fly-by-Wire	s	+	+	\
10 Lower Drag	+	-	-	\
11 Higher Lift	s	s	-	\
12 Higher Angle Rate of Climb	s	s	s	\
13 Maneuverability	-	-	-	\
14 Longer Design Life	s	s	s	\
15 Manufacturing Cost	-	+	+	\
16 Operation Cost	-	+	+	\
Total Positives (+)	3	3	4	0
Total Negatives (-)	9	5	9	0
Net	-6	-2	-5	0

Table 3.4: Third Iteration

Table 3.4 shows that the team included a net value for determining if one design had an overall advantage for this iteration. Don Clausing advises against creating a score for any given concept when using Pugh's method [3.1], but the team felt that this iteration served mainly to compare what it thought would be its best design to some previous ideas. In this way it could be certain its core concept would be the best to complete the mission. The net

results seemed to support the idea that the team should work toward a canard design, as no concept possessed a net advantage over it.

While the team's Pugh analysis produced the canard design as the potential best concept for the Metro-Scout design, it leaves open room for design modifications and improvements. The team may update the matrix at some point during the design should new information become available that may give another design aspect an advantage in a given category. Again, the end goal of the Pugh method involves producing the best overall concept, and in a changing market and design environment, the requirements of the aircraft may change over the course of its development.

3.3 Selected Concept

Team 4 has selected the single vertical tail canard pusher-prop aircraft concept (concept VII) to be the most viable solution for the mission engineering requirements, based on the results from the use of Pugh's method of concept selection.

Shown below is a walk-around view of the selected concept, detailing the internal and external layout of the Metro-Scout. (Please note that the Metro-Scout will have a fixed tricycle landing gear set-up, but that it is not depicted on the CAD walk-around view below as the gear itself has not been designed yet. Also, the mounts for the internal components will not be attached to the fuselage skin in the final design, and only appear to be so as the final conceptual structural layout has not been finalized by Team 4 yet.)
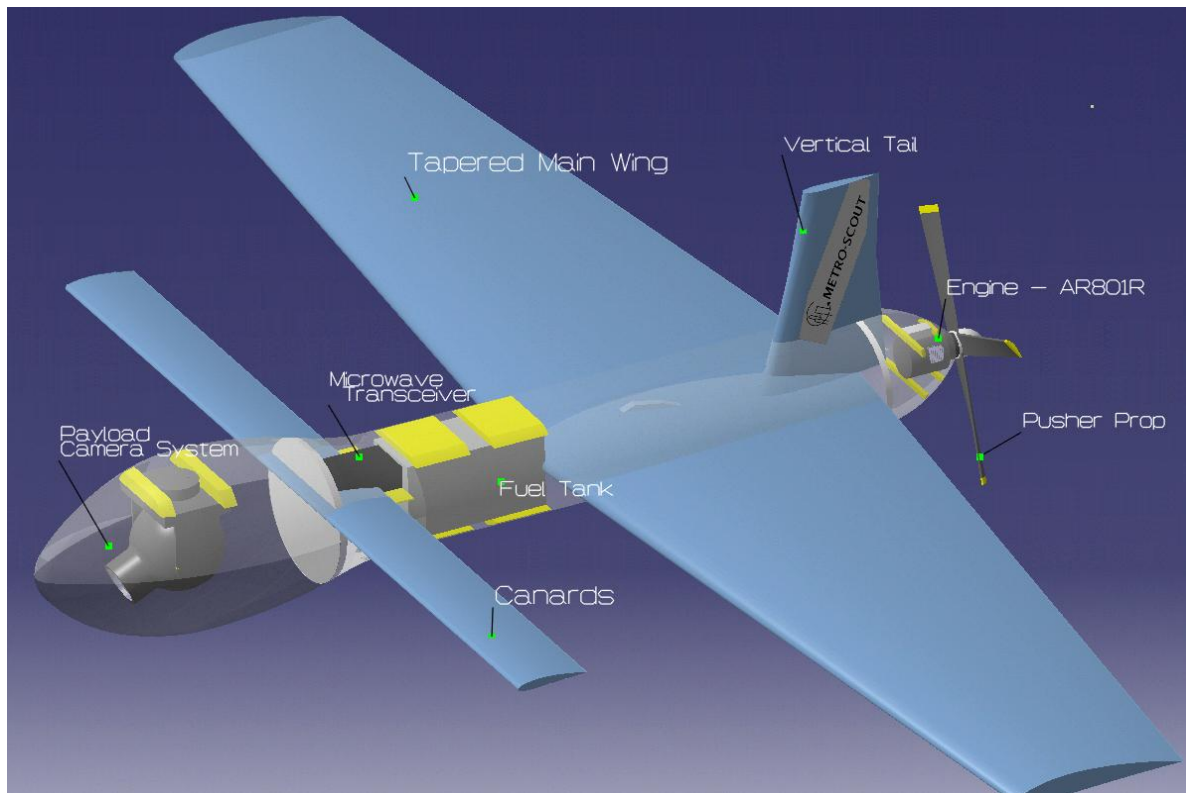
Figure 3.1: CAD walk-around image of the Metro-Scout concept - Note the Canards and Pusher Prop

The external layout of the Metro-Scout design is detailed on page 33 and the internal layout is detailed on page 36.

Team 4 has listed the specific plus-points and challenges associated with using a pusher-prop and canards in the following sections.

Use of a Pusher Prop: Highlights and Discussion:

Team 4 has elected to use a pusher-prop on the Metro-Scout design for the following reasons:

(1) *Visibility*: A tractor prop design would place the rotating propeller directly in the view-frame of the camera system and inhibit the visibility of targets that the camera was trying to track. A pusher-prop design places the propeller at the rear of the fuselage and out of the way of both the pilot and payload cameras.

(2) *Slipstream Effect:* The prop-wash coming off of a forward mounted propeller causes a number of undesirable effects on the wings, tail and control surfaces. This is

especially noticeable for canards where sudden changes in the engine throttle setting have been known to cause stalls, violent pitching motions, and even fatal crashes due to the slipstream effect. Changes in the throttle setting cause a noticeable difference in the velocity of the propeller slipstream that affects the control surfaces, and in turn causes the aircraft to experience distinctly observable pitch and yaw changes during power changes. This effect is summarized below in figure 3.2.

"SPIRALING SLIPSTREAM UNDER AND AROUND AIRCRAFT"

**Figure 3.1: Slipstream effect on a Cessna 172 (Image Source:
http://www.computerpilot.com/resource/files/samples/sampleArticle542.pdf)**

(3) *Exposed Area & Resultant Drag:* A mid-fuselage mounted engine-propeller arrangement such as observed in aircraft like the Lake Renegade (pictured below) adds a large amount of exposed area to the free-stream which tremendously increases drag. Such an arrangement is useful primarily for keeping the prop completely out of reach of the ground or in the case of sea-planes, out of danger of hitting water. A pusher-prop is relatively efficient in the aspect of exposed area and drag – as the airflow can be made to remain relatively laminar over the fuselage leading into the propeller and the usually flat non-streamline surfaces of the engine housing are not exposed to the free-stream. Additionally, a fuselage-mounted pusher prop reduces the wetted area of the aircraft by shortening the fuselage. [2.1] Team 4 will size the landing gear on the Metro-Scout to ensure adequate ground clearance for landing and take-off.

Figure 3.2: Mid-Fuselage Mounted Engine on a Lake Renegade (Image Source: www.teamlake.com)

(4) _Reduced Aircraft Skin Friction Drag:_ A pusher prop design allows the fuselage, wing, canards and tail to fly in a region of undisturbed air. Not flying in the prop-wash created by a tractor prop configuration reduces the aircraft skin friction coefficient, and so, the overall drag of the aircraft. [2.1]

(5) _Reduced Cabin/Payload Bay Noise and Vibrations:_ In the current configuration of the Metro-Scout, the payload is at the opposite end of the fuselage from the engine – this serves the benefit of reduced vibrations and engine noise being felt in the payload compartment. The cameras and avionics are expensive, sensitive equipment, and a pusher-prop design goes a long way toward increasing the life-span and decreasing the maintenance costs of the payload equipment. [2.1]

(6) _Canard-Pusher Combination Advantage:_ Canard aircraft are usually designed with a pusher-prop because of the additional benefit of having a shorter tail arm as compared to an aft tail. [2.1]

Naturally, as with any type of design, there are a unique set of challenges associated with a pusher-prop design. These are listed below:

(1) _Ground Clearance:_ Most notably, pusher-prop designs need longer landing gear to ensure adequate ground clearance for taxi, take-off and landing. Soft-field and rough field landings are a special challenge for pusher-props as dirt, rocks or turf can get kicked into the propeller blades. It is Team 4's decision that the Metro-Scout cannot and does not need to, given the nature of its customers, be certified for types of operations requiring rough field landings where a risk of FOD (foreign object damage) into the propeller blades can occur. [2.1]

(2) *Reduced Efficiency:* In pusher-prop designs, the propeller acts in a region of disturbed flow coming off of the fuselage, wings and canards, and so, has a certain amount of reduced efficiency. [2.1] For the Metro-Scout design, an attempt will be made to keep the flow coming off the fuselage relatively laminar. However, given the relative parasite drag-savings gained by not having prop-wash act on the fuselage, canards, and wings, the reduction in propeller efficiency can be negated with the right design.

(3) *Engine Cooling:* Due to the location of the engine, engine overheating is an issue that a number of canard pusher-prop designs have had to overcome. Team 4 will look into positioning air inlets on the fuselage specifically for engine cooling in locations of uninterrupted airflow where attitude changes will not result in significant flow-rate changes.

(4) *Aural Signature:* Pusher-prop designs have a notoriety for being noisy compared to conventional tractor-prop designs. This is primarily due to the engine exhaust flowing through the propeller blades generating a characteristic whine. Additionally, airflow shearing off discontinuities in the fuselage, control surfaces, turbulent air coming off the wings can contribute to an increased noise signature as it passes through the propeller. Given that the Metro-Scout will be operated over metropolitan areas, reducing propeller noise is a legitimate design objective. Team 4 will look into ways to redirect engine exhaust away from the propeller blades such as through exhaust pipes that vent out the trailing edge of the vertical tail or the wings. Additionally, every attempt will be made to keep flow laminar over the fuselage by minimizing protrusions or discontinuities in the fuselage.

Use of Canards: Highlights and Discussion

On an intuitive level, from an engineering standpoint, Team 4 can subjectively say that a Canard aircraft design, if done right, can give the Metro-Scout product advantages in terms of maneuverability, safety, fuel-efficiency, and weight & drag-savings that far outweigh the potential disadvantages in airframe complexity, and increase in time and cost for design, analysis, optimization and flight-testing. To further elaborate on this, table 3.5 below highlights the following items:

(1) Positives and negatives that Team 4 has established for a Canard aircraft as it relates to the specific mission capabilities required for the Metro-Scout Product

(2) Some historically observed trends for advantages and disadvantages of Canard type aircraft

Typical Canard Aircraft Characteristics	
Advantages	Disadvantages/Challenges
(1) Good Stall Characteristics/Can prevent stall (2) Pusher-Prop → Packaging/Assembly can be much simplified (3) Canard lift can be made to compliment main wing lift (4) Fuselage supported in two places – Some weight savings (5) Sometimes more useful range of c.g. (6) Can have added Maneuverability (7) Can have added fuel-efficiency	(1) Canard Sizing is highly critical – small changes can affect performance (2) Downwash/Upwash effects on the main wing from the canard (3) Susceptible to Deep Stall if pilot/operator over-maneuvers airframe (4) Small moment arm of Canard – leading to larger canard area (5) Added time for wind-tunnel analysis and flight-testing

Table 3.5: Observed Advantages and Disadvantages of using Canards in Aircraft Design [2.1], [2.3]

As mentioned earlier, how much each of these potential advantages and disadvantages impact aircraft performance characteristics are dependent uniquely upon the exact nature of the Metro-Scout design. With a properly designed aircraft that incorporates design elements that build upon the lessons learnt from available literature on previous Canard designs, Team 4 believes that the Metro-scout design can be quite successful and virtually problem-free. Team 4 has already conducted preliminary aerodynamic and stability analysis into the Metro-Scout canard concept. Current estimates indicate that a high static-margin on the order of 12-15% can be achieved using canards with a span of 10-14 feet, and a chord length of 1 foot. Currently, the canards complement the lift generated by the main wing to achieve greater efficiency. The aim is to counter the reduction in lift on the main wing by putting in some lift on the canard. Also, the placement of the canards and the main wings

reduce redundancy in structural load bearing elements. For instance, the structural members holding the canard to the fuselage also partially bear the weight of the payload and the front of the aircraft. Similarly, the engine, the vertical tail and the main wing share a rigid common root support-structure that connects them to the rest of the fuselage.

Team 4 will continue to evaluate the sizing of the canards on the Metro-Scout to achieve the most efficient balance between performance, stability and fuel-efficiency for the aircraft.

In addition, Team 4, as a result of its experience thus far in the aerospace culture, has noted the inherent culture of resistance in both customers and manufacturers in the commercial aircraft market to the mass-production of non-conventionally designed aircraft. Team 4 considers that the use of canard technology in aircraft has reached a sufficient level of technology maturity to enable both customers and the industry to accept that the performance, reliability, manufacturability and financial viability are comparable to that of a conventional aircraft design that would perform the same function.

A lot of this level of technology maturity, at least in the modern era, can be attributed to the work of noted aircraft engineer and designer Burt Rutan. The use of canards in Rutan's designs incorporates elements of design simplicity, cost-effectivity, safety & maneuverability, and high performance. The Rutan-designed Long-EZ and Proteus aircraft (pictured below) have achieved high endurance times far beyond other aircraft in their respective classes as a result of their effective use of canards. [2.3]

Figure 3.3: Proteus Aircraft (Scaled Composites/Northrop Grumman), (Image source: NASA)

Team 4 has noted that manufacturing and production times do not seem to be significantly affected either positively or negatively by going with a Canard type design. Delays and problems with the manufacturing process in historical examples of the development of some canard aircraft could be attributed to inaccurate tasking, confusion among manufacturing personnel resulting from miscommunication of procedures, and in one unique case involving a Japanese/German fighter design- the end of World War II. But clearly, these are problems that are not intrinsic to the use of canards.

3.4 External Layout
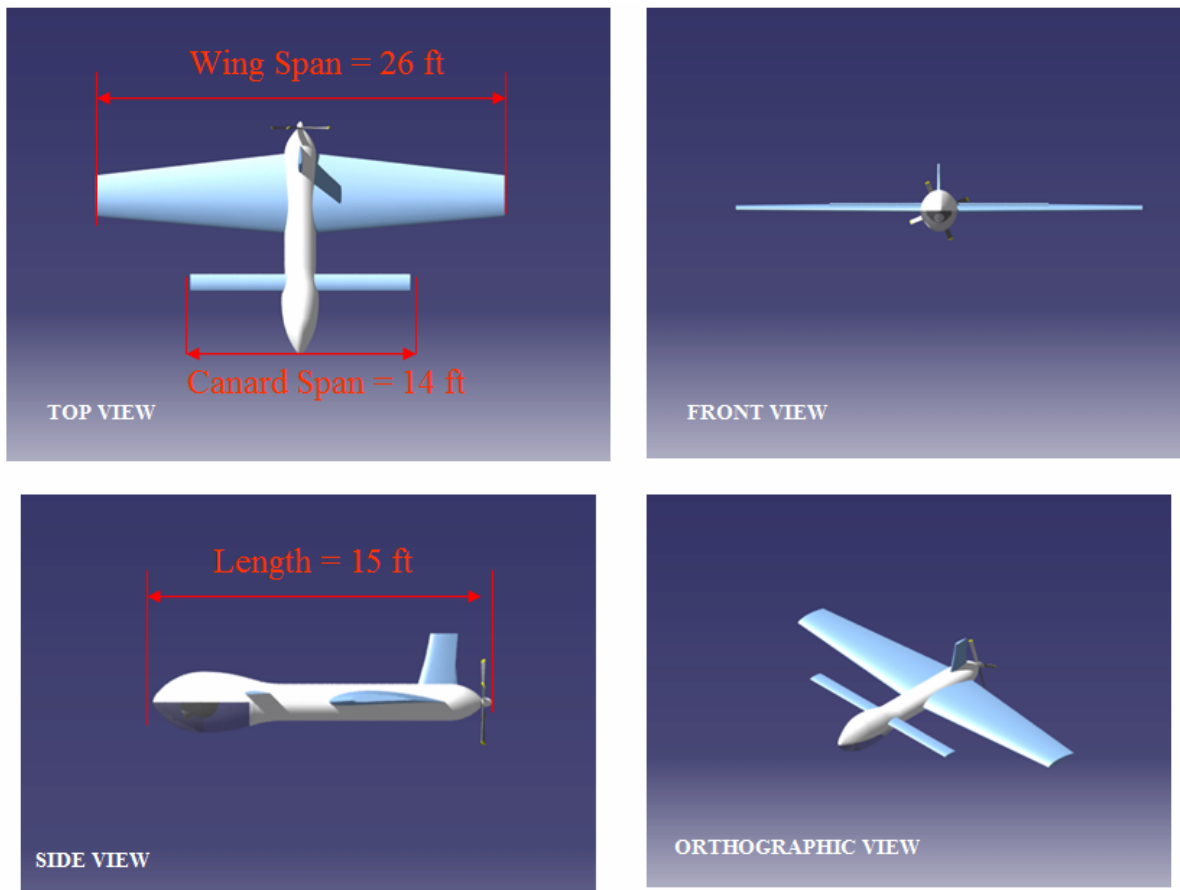
Figure 3.4: CAD 4-view of the External Layout of the Metro-Scout

The Metro-Scout is sized based primarily on the following requirements:

> (1) To allow all internal equipment such as payload, engine, avionics, and structure to be mounted safely and with ample room to allow easy access for maintenance, and freedom of interference from neighboring equipment.
>
> (2) To allow the positioning of the wings, canards, vertical tail and control surfaces to achieve the desired levels of stability, maneuverability, and controllability in all flight conditions.

Figures 3.5 above and 3.6 below show some initial external dimensioning on the Metro-Scout.
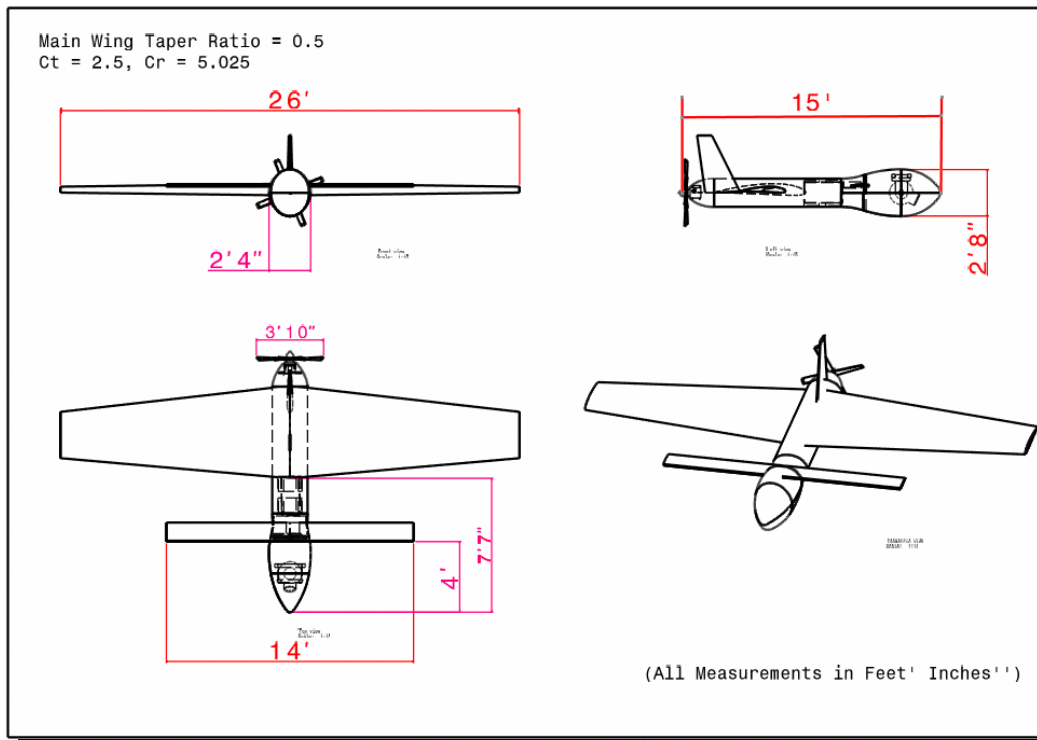
Figure 3.5: CAD Sketch of the Metro-Scout with additional dimensioning and internal cutaway

The main wing, as with most canard aircraft is placed toward the rear of the fuselage in order to position the center of gravity in an optimum location. The engine and propeller are located directly behind the main wing box. In addition, the vertical tail is placed directly behind the main wing box. An additional benefit of this positioning is that the engine, the

vertical tail, and the main wing share a rigid common root support-structure that connects them to the rest of the fuselage.

The main wings are not swept back because the payload weight in the nose provides sufficient ballast to maintain the c.g. within controllable limits so that the engine weight cannot tip the airplane over during rotation for takeoff or landing. This negated the need for wing sweep to move the engine closer to the aircraft center of gravity.

Currently the main wing span is 26 feet, with a root chord of approx. 5 feet, and a tip chord of 2.5 feet. The sizing of the wing is based on initial aerodynamic analysis that Team 4 conducted, which is detailed in section 5 of this report. Based on the requirements for stability and controllability, the canard was placed at a distance of 4 feet from the nose of the fuselage. The canard span is 14 feet from tip to tip. It is based on a rectangular planform with a chord of approximately 1 foot.

3.5 Internal Layout

The fuselage of the aircraft was designed in three separate parts, each with a different driving force behind the design. The position of the components of the aircraft (payload, canard, transmitter, fuel tank, wing, tail and engine) had already been roughly chosen, so the fuselage was split up according to which components it would need to house. The front section houses the payload and the canard and requires a "bubble" of glass on the belly so that the cameras will not add to drag but still be able to function. The mid section houses the fuel tank and the transmitter and the last section houses the wing box and tail structure.

The front of the fuselage needs to be wide enough to accommodate a 24 inch x 24 inch cube which represents the area in which the largest camera can move. Giving the cube a 2 inch buffer from any point on the fuselage ensures that any vibrations will not cause the camera to hit the glass bubble. The 8 inches of distance between the top of the camera mount and the top of the fuselage allows sufficient space for both mounting structures and wiring. The canards are also placed in this section of the fuselage, located behind the payload. The aerodynamic center of the canard is 3.7 feet behind the nose of the aircraft.

The size of the fuel tank was the driving force behind the design of the next section of the fuselage, between the bubble and the wing. The fuel tank needs to be located outside and in front of the wings because of the wing box, the small thickness of the wing, and in order to move the center of gravity forward. A short and wide tank was chosen so that as the fuel level lowers and the fuel has more freedom of movement, it will not change the c.g. significantly during maneuvering. Also, the fuselage needed to be as skinny as possible in order to reduce surface drag. The final tank size was 12.12 inches x 26 inches x 14inches. This fits into the midsection of the fuselage with a 7 inch clearance on each side and a 5 inch clearance on the top and bottom. This is enough space for structures to mount the fuel tank. The microwave transmitter was also placed in this section, just forward of the fuel tank. This 12 inch x 9inch x 4inch box weighs approximately 11 pounds and will share a mounting platform with the autopilot controller, which is of negligible size and weight.

The last section of the fuselage, which will extend from behind the fuel tank to the trailing edge of the tail will house the wing box and tail structure. Neither of these has been designed yet but they are anticipated to require that the size of the fuselage will be larger than the fuselage surrounding the fuel tank and microwave transmitter. Though it is modeled as an inboard engine in the Catia model, a decision has been made to mount the engine outside of the fuselage in order to use the air to cool it.

Figure 3.7 is a wire view of the Metro-Scout. This view shows the dimensions of the payload pay and the fuselage. The side view of the aircraft shows the distance from the nose to the payload, canard, transmitter, fuel tank, wing and the total length of the aircraft. Note: In the final design the transmitter will be moved down to make room for the canard.
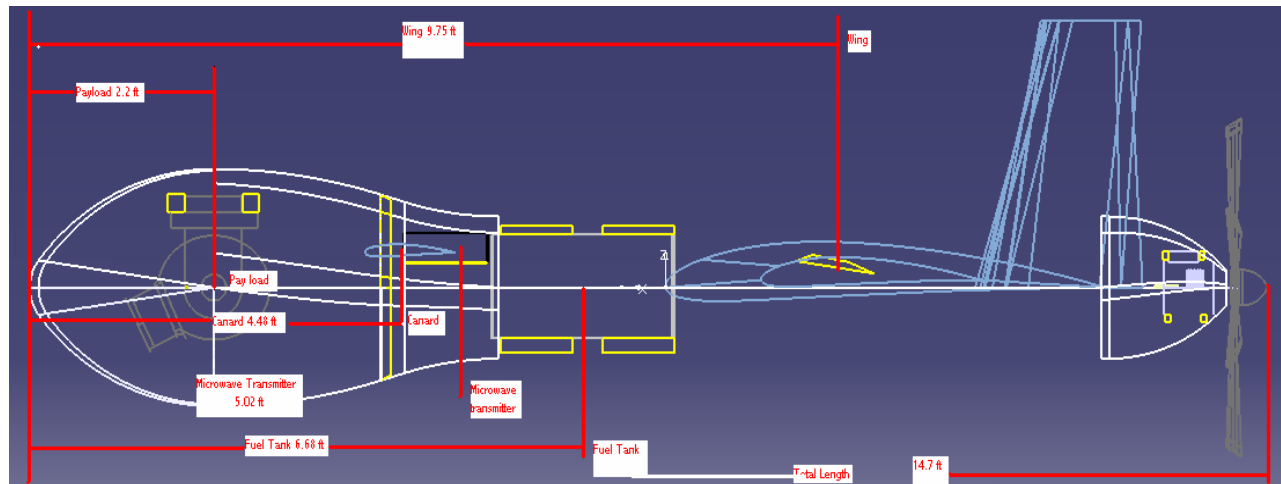
Figure 3.7 Inboard Layout

The team is not at the point in the design where internal fuselage structures have been designed. That is the reason that the Catia model shows the representations of the component mountings as being attached to the skin of the fuselage. In future steps, ribs will be placed to give the fuselage the appropriate strength, as well as provide the structure needed to support the component mounts. Also being developed is the wing box and tail structure.

3.6 Payload Integration

Different payloads are required for the different missions designed for the law enforcement agencies and the news agencies. These payloads were created based on the concept of operations described above and the different customer attributes requested.

Table 3.6 lays out exactly what pieces of equipment are compiled to make up the payload package that will be sold to law enforcement.

Package	Payload	Weight(lb)	Dimensions(ft)
Police package	Radar gun	1	0.5 x 0.19 x 0.45
	Camera gimbal	51	.92 x 1.25
	ThermaCAM SC3000	7	mounted on gimbal
	Sony DSR-PD150 (video cam)	3.1	mounted on gimbal
	Canon powershot S3 IS (still camera)	0.9	mounted on gimbal
	Canon lens f/4.5-5.6 II USM	0.7	on camera
	Autopilot	0.2	.34 x .17 x .14
	Total weight	64	

Table 3.6:Payload Package for Law Enforcement[3.2],[3.3],[3.4],[3.5],[3.6],[3.7],[3.8]

During highway patrols for speeding vehicles, the Metro-Scout will fly at the speed limit set for the highway and any car moving faster than the UAV will trigger the radar gun to record the exact speed of the speeding vehicle. This in turns triggers the still camera to snap a picture of the vehicle's license plate. Law enforcement officers can then issue the violators a ticket and mail it to them.

In search and rescue operations, the video camera, infrared and still camera will work in tandem with one another. If the infrared camera detects a possible target, the video and still cameras will be used to positively identify the target. These images are then sent back via live feeds through a transmitter.

The radar gun has an accuracy of 1.25 miles per hour and is able to measure a target speed moving in a co-direction takes place if the speed difference is varied from 2.5 up to 62 miles per hour. It is also not important where the target is located – in front of UAV is or behind the UAV, the UAV catches up with target or the UAV is left behind target - in any case the correct evaluation of a target speed is guaranteed by Semicon. This lightweight radar gun of less than 1 pound will be placed on the UAV and feed back information on traffic violators.

The Camera gimbal has a 4-axis gyro stabilized video system. It is able to rotate 360 degrees and track stationary and moving targets from up to 3000 feeht. [3.3] The camera operator can control the gimbals' system which then transmits the video feeds and still images through microwaves back to the ground.

The ThermaCAM is an infrared camera coupled with its software can provide live feeds of an extensive temperature range. It is able to measure extremely small and distant targets with great accuracy (±1%) and high resolution. [3.4] This will assist law enforcement in criminal pursuit during the day and even at night. In the event that the suspect is hidden from the regular view of a regular camera, the infrared can still detect the heat signature of the suspect. This infrared camera is also relatively light at seven pounds, providing an additional capability which aids the capture of criminal suspects.

Most importantly, a video camera is also mounted on the gimbal. The Sony DSR-PD150 has a build in image stabilizer with a 12 X optical and 48X digital zoom. [3.5] This camera will be able to provide close up aerial videos from the air. This camera is also very light weighing only 3.1 pounds.

A high resolution still camera is also essential for law enforcement agencies. The Canon powershot S3 IS will be equipped with a 50-200 millimeter lens that will be able to take high resolution still images of license plate numbers from up to a distance of 3000 feet. [3.7] This camera can also be used by law enforcement to take high quality pictures of evidence against fleeing suspects.

The autopilot's software for the UAV is capable of flying at a Maximum Altitude of 16,000 feet above sea level and a maximum airspeed of 150 miles per hour. It comes with a transmitter to broadcast airspeed, pressure and temperature to the ground in compliance with FAA regulations.

The payloads for the news stations are as follows:

Package	Payload	Weight(lb)	Dimensions(ft)
News Station/filming package	Cineflex V14	67	1.21 X 1.63 X 1.63
	Autopilot	0.1875	0.34 X 0.17 X 0.14
	Total weight	67.1875	

Table 3.7:Payload Package for News Agency [3.8],[3.9]

The camera for the news station allows for high definition live video feeds. This camera weighs more than the entire payload for the law enforcement as it is a high definition filming camera mounted on a gimbal, but the 67lbs includes the weight of the gimbal. The Cineflex camera is also currently mounted on helicopters and also used for filming movies. The built in wide angle view and infrared cameras allow for filming at all times of the day. Lastly, the Cineflex also has a 25X zoom enabling aerial footages to be filmed from up to 3000 feet. [3.9]

4.0 Constraint Analysis

4.1 Constraints

The performance analysis, in most cases, answers the question of whether a particular aircraft design will meet a customer's needs. The process of constraint analysis is to narrow down the choices of the many interrelated variables to control and make choices to which to design an aircraft such that it will have the desired performance capabilities. Constraint analysis provides ranges of values for an aircraft concept's take-off wing loading and take-off power loading, which allow the design to meet specific performance requirements.

The constraint analysis is based on a modification on equation 4.1 for specific excess power

$$\frac{T}{W} = \frac{D}{W} + \frac{1}{V}\frac{dh}{dt} + \frac{1}{g}\frac{dV}{dt} \qquad\qquad 4.1$$

In equation 4.1, T/W is the thrust to weight ratio, D is drag, V is velocity, dh/ht is the altitude derivative and dV/dt is the velocity derivative. By substituting equations 4.2, 4.3, 4.4 and 4.5 into equation 4.1, the new constraint equation is stated in equation 4.6.

$$T = \alpha T_{SL} \tag{4.2}$$

$$W = \beta W_{TO} \tag{4.3}$$

$$C_L = \frac{L}{qS} = \frac{nW}{qS} \tag{4.4}$$

$$D = C_D qS = (C_{D0} + \frac{C_L^2}{\pi A \operatorname{Re}})qS \tag{4.5}$$

$$\frac{T_{SL}}{W_{TO}} = \frac{\beta}{\alpha}\left\{ \frac{q}{\beta}\left[\frac{C_{D0}}{(W_{TO}/S)} + \frac{1}{\pi A \operatorname{Re}}\left(\frac{n\beta}{q}\right)^2\left(\frac{W_{TO}}{S}\right) \right] + \frac{1}{V}\frac{dh}{dt} + \frac{1}{g}\frac{dV}{dt} \right\} \tag{4.6}$$

In equation 4.2, α is the thrust lapse ratio which depends on the density ratio ρ/ρ_{SL}. In equation 4.3, β is the weight fraction for a given constraint. This fuel fraction is necessary because the weight loss from the fuel has to be taken into consideration at every moment throughout the flight. Equation 4.4 is the equation for the lift coefficient. Equation 4.5 is the drag equation based on the lift coefficient found in equation 4.4. Equation 4.6 is the newly defined power equation for take-off weight. [2.1]

4.2 Takeoff Constraint

While equation 4.6 models in-flight performance, the takeoff constraint requires a different equation. Assuming $V_{TO} = 1.2V_{stall}$, equations 4.7, 4.8, and 4.9 are written below.

$$V_{TO} = 1.2\sqrt{\frac{2W_{TO}}{\rho S C_{L\max}}} \tag{4.7}$$

$$t_{TO} = \frac{1.2W}{\{g[T - D - \mu(W_{TO} - L)]\}^2}\sqrt{\frac{2W}{\rho S C_{L\max}}} \tag{4.8}$$

$$s_{TO} = \frac{1}{2}at_{TO}^2 = \frac{1.44W_{TO}^2}{\rho S C_{L\max}g[T - D - \mu(W_{TO} - L)]} \tag{4.9}$$

Rewriting equation 4.6 using equations 4.7, 4.8 and 4.9, equation 4.11 is the new power equation in terms of power loading, equation 4.10, and wing loading.

$$\frac{P}{W_{TO}} = \frac{T_{SL}}{W_{TO}} \left(\frac{V_{TO}}{550\eta_p} \right) \qquad 4.10$$

$$\frac{T_{SL}}{W_{TO}} = \frac{1.44\beta^2}{\alpha\rho C_{L\max} g s_{TO}} \left(\frac{W_{TO}}{S} \right) + \frac{C_{D0}q}{\beta(W_{TO}/S)} + \mu \qquad 4.11$$

The unit of power in the above equation is horsepower. These equations also assume that lift is approximately zero prior to rotation. [2.1]

4.3 Sustained Turn Constraint

Maximizing thrust loading and lift to drag ratio (L/D) maximizes the load factor in a sustained turn. At max L/D, the coefficient of drag is C_{D0}, therefore deriving equation 4.12.

$$\frac{W}{S} = \frac{q}{n} \sqrt{\pi A \operatorname{Re} C_{D0}} \qquad 4.12$$

Equation 4.12 is the wing loading equation for the max range and max propeller loiter for a propeller aircraft. This equation proves that as weight reduces due to fuel burned, the wing loading also decreases during cruise. Optimizing cruise efficiency while wing loading is decreasing requires the reduction of the dynamic pressure by the same percent as seen in equation 4.12. The concept of max L/D and the above wing loading equation yields equation 4.13; the available thrust equation. [2.1]

$$\frac{T}{W} = \frac{qC_{D0}}{W/S} + \frac{W}{S} \left(\frac{n^2}{q\pi Ae} \right) \qquad 4.13$$

4.4 Landing Constraint

The landing constraint determines the maximum value of wing loading of the UAV. The maximum wing loading bounded by the landing constraint is calculated from the landing constraint equation below.

$$\frac{W}{S} = \frac{d_{land}\rho C_{L\max} g\mu}{1.68\beta} \qquad 4.14$$

In equations 4.14 d_{land} is the landing distance, μ_{land} is the friction coefficient when landing, β is the landing weight fraction (W_{land}/W_o).

4.5 Constraint Results

By running MATLAB code developed by team members, the group determined a design point for power loading and wing loading. Figure 4.1 shows this design point in terms of a specified power loading and wing loading value. [2.1]
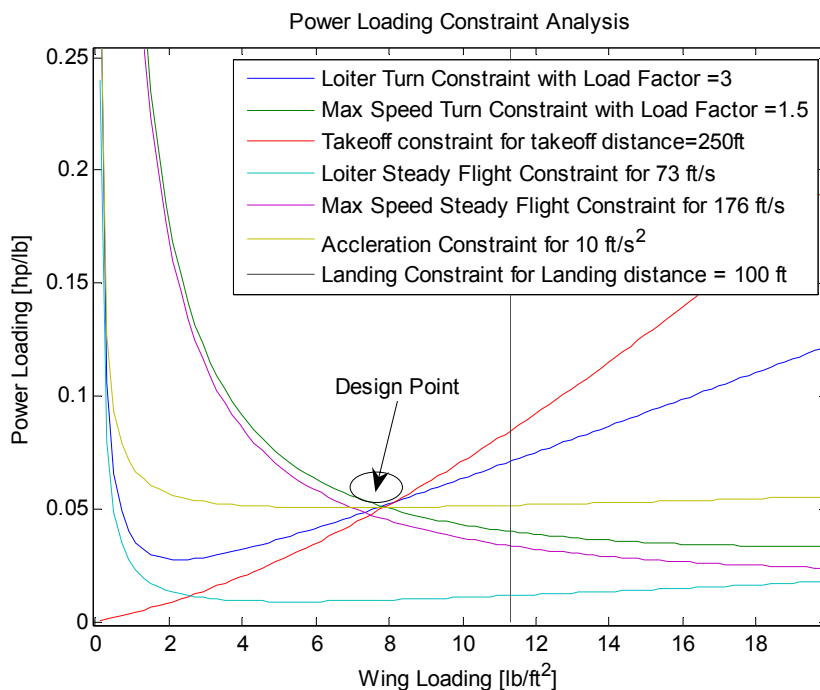
Figure 4.1: Power Loading Constraint Analysis

This point represents a ratio of power loading to wing loading that best blends the loiter turn, max speed turn, and takeoff constraints. It does not necessarily optimize any of these constraints, but rather suggests a point where changing one constraint would adversely affect another. Table 4.1 below, shows the optimum design point.

Power Loading	0.053 hp/lb
Wing Loading	7.8 lb/ ft^2

Table 4.1: Power Loading and Wing Loading Data

The driving constraints were the acceleration and the max-speed turn load factor constraints. The driving constraints determined the power loading and wing loading of the UAV. The non-driving constraints are also shown in figure 4.1 to demonstrate the capability of the UAV.

	Mission Requirement	Value Achieved
Max-speed Turn Load Factor	1.5g	1.5g
Acceleration for loiter to max speed	10 ft/s^2	10 ft/s^2
Take-off distance	1500 ft	250 ft
Loiter-speed Load Factor	2.5g	3.0g
Landing Distance	1500 ft	100 ft

Table 4. 1 : Performance Capability

4.6 Sizing

Sizing is the process to determine how large the aircraft must be to carry enough fuel and payload to be able to loiter for up to five hours and to take surveillance for new agencies and law enforcement. A crude estimate of the maximum L/D is obtained. Specific fuel consumption is dependent on the engine chosen for the UAV which is discussed in section 6. SFC ($C_{hpb)}$) was taken to be 0.52 and 0.56 lb/hp/hr for cruise and loiter respectively [5.1]. C_{D0} was obtained from the wetted area calculated for the estimated shape of the UAV. Since empty weight is calculated using a guess of the takeoff weight, it is necessary to iterate towards a solution. The initial empty weight fraction was obtained from regression analysis on historical similar UAVs. The empty weight is an estimation of combination of all component weight uncertainties. Equation 4.15 is the actual equation used to determine the empty weight fraction of the Metro-Scout.

$$\frac{W_e}{W_0} = -0.1 + 0.75 W_0^{-0.13} AR^{0.06} Powerloading^{0.08} Wingloading^{-0.05} V_{MAX}^{0.21} \qquad 4.15$$

The team has developed a MATLAB program to calculate the total takeoff weight.

	Value Inputted
Power loading	0.0525 hp/lb
Wing loading	7.8 lb/ft^2
SFC for cruise	0.52 lb/hp.hr
SFC for loiter	0.52 lb/hp.hr
AR	13

L/D	13
C_{D0}	0.0239
η_p	0.80
Oswald's efficiency	0.8

Table.4.2 : Inputs of Sizing Program

4.7 Fuel Fraction for Cruise and Loiter

The gross weight equation is based on the fuel fraction and the empty weight fraction. Both of these equations are based on L/D. The L/D equation shown in equation 4.16, is derived on the premise that C_{D0} is .0239, AR is 13, and e is 0.75. This equation is also under the assumption that V_{loiter} is 73ft/s and V_{cruise} is 176 ft/s.

$$\frac{L}{D} = \frac{1}{\left[\dfrac{qC_{D0}}{(W/S)} + \dfrac{W}{S} \dfrac{1}{q\pi A \,\mathrm{Re}} \right]}$$

4.16

The fuel fraction and weight equations derived from the Breguet equation for cruise and loiter, used to find the gross weight, are shown in equations 4.17 and 4.18 respectively.

$$\frac{W_i}{W_{i-1}} = \exp\left[\frac{-RC_{bhp}}{550\eta_p (L/D)} \right]$$

4.17

$$\frac{W_i}{W_{i-1}} = \exp\left[\frac{EVC_{bhp}}{550\eta_p (L/D)} \right]$$

4.18

In these equations R is range, E is endurance, C_{bhp} is the specific fuel consumption for propeller aircraft. η_p is the propeller efficiency. The i index in the above equations is the segment number. In any given flight there are multiple segments. For example, in a normal flight, the loiter segment would by i=4 after the take-off (i=1), climb (i=2), and cruise (i=3).

The aircraft weight is calculated throughout the mission. For each segment the aircraft weight is reduce by fuel burned. Total fuel burned is calculated throughout the mission and found by summing the weight fractions from each flight segment in equation 4.19.

$$W_{fuel} = 1.06\left(\sum_{i}^{x} W_{fi}\right)$$ 4.19

In equation 4.19, 6% of extra fuel is added for landing, takeoff, taxi and reserve. Equation 4.20 is the takeoff weight equation.

$$W_0 = W_{pay} + W_{fuel} + \left(\frac{W_e}{W_0}\right)W_0$$ 4.20

This equation is a summation of the different weights calculated from the various fuel fractions. [5.9]

Using data collected from the above analysis, table 4.4 is a compilation of the initial sizing results.

Total Aircraft Takeoff weight	603 lb
Fuel Weight	116 lb
Payload Weight	63.1 lbs
Aircraft Inert Weight	424 lb
Power Required	31 HP
Wing Area	77 ft^2

Table 4.4: Sizing Data

4.8 Carpet Plot

The carpet plot shows a direct relationship between gross take-off weight, and a range of wing loading and power loading. It also provides estimates of the gross take-off weight with variants in wing loading and power loading. The carpet plot is generated by inputting a range of wing loading and power loading values into the sizing MATLAB code developed by the team.
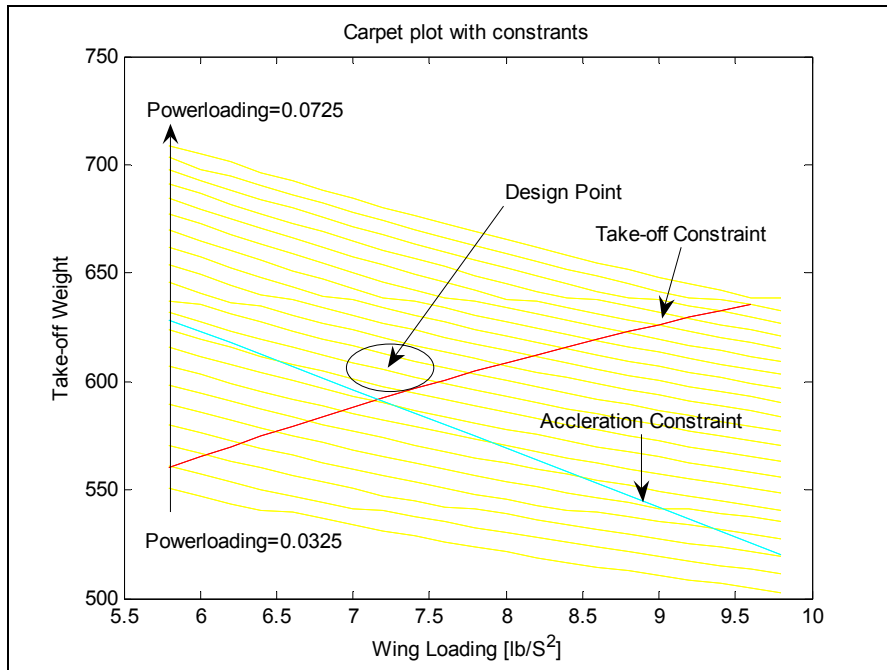
Figure 4.2 Carpet Plot

4.9 Aspect Ratio Analysis

By generating carpet plot for a range of aspect ratios, and taking the lowest talk-off gross weight for each aspect ratio, a plot of the take-off gross weight versus aspect ratio is shown below.
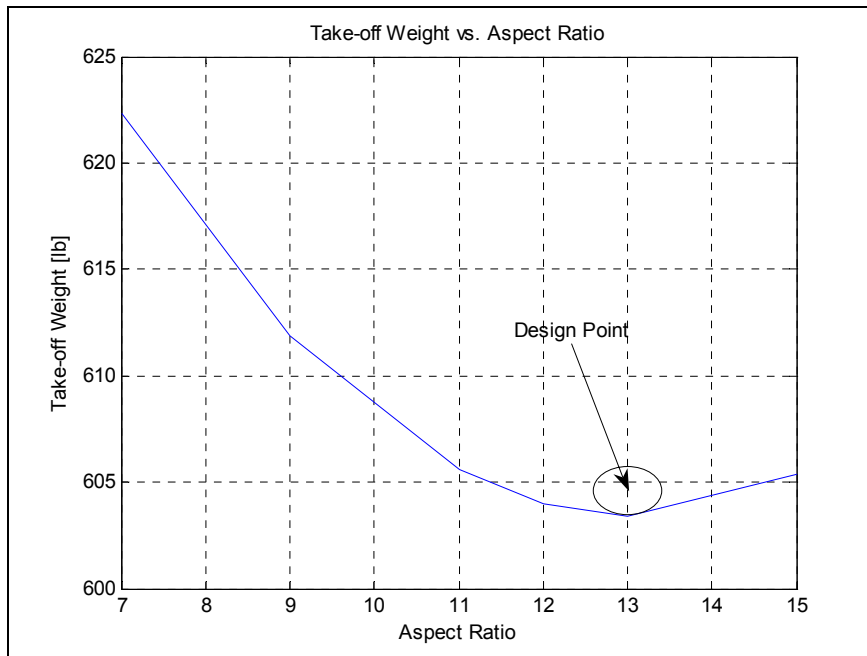
Figure 4.3 Take-off Weight versus Aspect Ratio

The plot shows the optimal aspect ratio at 13. Currently the team does not feel comfortable with this high aspect ratio and is working with the weight equations to get back to a more suitable number.

For the purposes of initial sizing and concept selection, Team 4 selected an aspect ratio of 6.8 for the Metro-Scout main wing. The rationale behind this initial aspect ratio selection was that historically, general aviation and homebuilt aircraft have an average aspect ratio of 6.8. [Raymer, 2.1] Team 4 felt that the Metro-Scout UAV would most likely fit somewhere between those two categories of aircraft. However, in future analysis of fuel-savings, weight-savings, and structural analysis, Team 4 anticipates that the final aspect ratio selected will be somewhere in the 9-12 range.

5.0 Aerodynamic Analysis

5.1 Airfoil Selection

In selecting an airfoil, the aircraft design requirements must be found, such as how it should perform and how it should handle. In general, a higher section coefficient of lift (c_l) causes in a higher section coefficient of moment (c_m) during cruise. [1] As a result of this pitching moment, the canard must, in turn, provide necessary lift to balance the nose down effect which in turn leads to a higher trim drag.

From the customers and mission requirements, a loiter speed of 50miles per hour and maximum speed of 120 miles per hour were below 130 miles per hour at which NACA airfoils are proven to work. Because of this, the analysis was done using 4-digit NACA airfoils. [5.1] The 4-digit series was also chosen due to its small center of pressure movement across a large speed range. [5.1]

The main criteria of the airfoil selection were a high c_{l0} and a high c_{lmax} with c_l over coefficient of drag (c_{di}) and c_m as secondary requirements. This was because of the need for a high c_{l0} to cruise efficiently without requiring a larger planform area at the required loiter velocity of 50 miles per hour. A high c_{lmax} would provide a higher wing loading for a shorter takeoff distance and for a better sustained turn rate. [5.2] A low pitching moment close to zero about the aerodynamic center would lower trim drag induced by the canard.

This, however, can be adjusted by adding counter weights such as payloads or varying the location of the fuel tank in the fuselage to minimize this effect.

The analysis was done with varying camber, while the location of the camber from the leading edge remained constant at 40% chord length and the thickness remained at 12% chord length.

As the location of the camber from the leading edge increased, c_l increased, thus the location of the camber from the leading edge was picked to be as far back as possible. However, to maintain a small coefficient of moment, we need to keep the location close to the first quarter of the chord.[5.3] Therefore a compromise was reached in picking a camber at 40% chord length which has a reasonably low pitching moment and provides high c_l values.

When airfoil thickness increases, the c_l values increase. However, c_l values stop changing significantly after 12% thickness to chord for NACA 4-digit airfoils. [4] Since a greater thickness to chord ratio increases drag and the wings of the UAV are not going to store fuel, an airfoil thicker than 12% chord is not practical. Thus a thickness of 12% chord was chosen.

The following four graphs were plotted from the output of XFOIL. Assumptions made include a Reynolds number, Re, of a constant 2.3E5 and a Mach number, M, of constant 0.0663.

Plots of c_l versus alpha for five airfoils with increasing camber are shown in Figure 5.1. This graph allows us to identify the c_{lmax} of the various airfoils which is the maximum point for the five plots.
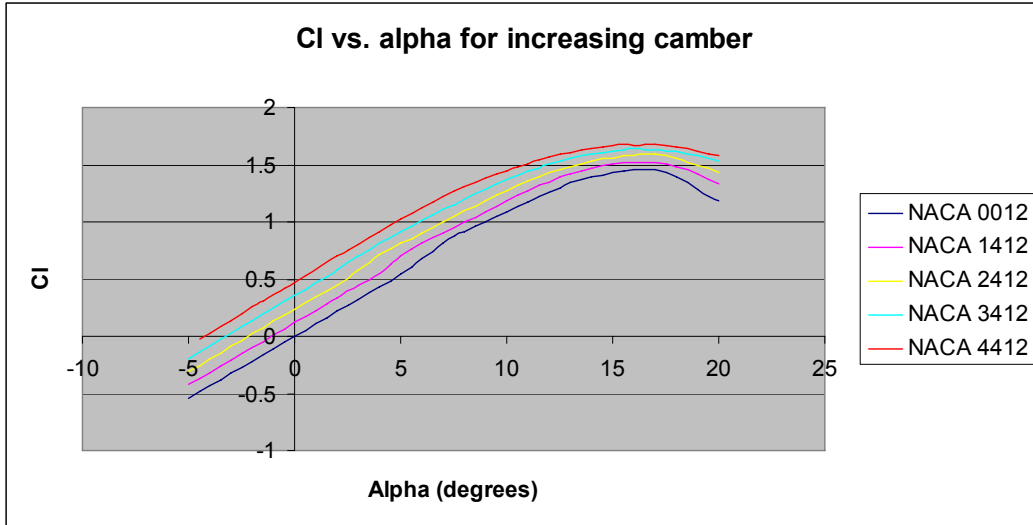
Figure 5.1 C_l versus Alpha for Increasing Camber

Figure 5.1 shows that an increased angle of attack increases the coefficient of lift. The maximum point of each line in the graph represents the c_{lmax}. The NACA 4412 has the highest c_{lmax}, 1.65 and cl0, 0.5.

Plots of c_m vs. alpha for five airfoils with increasing camber can be seen in Figure 5.2. These plots show the fluctuations in c_m as alpha is increased.
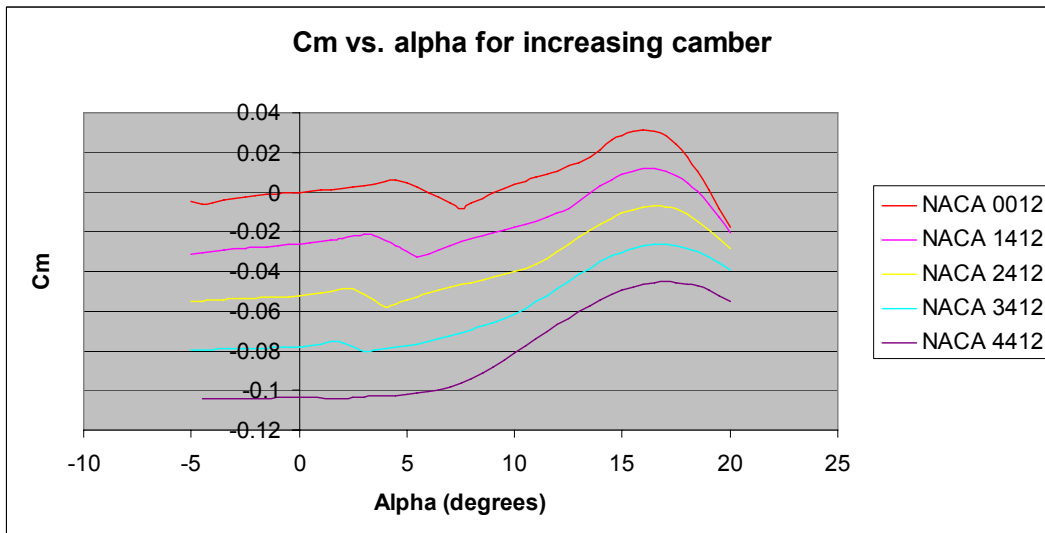
Figure 5.2: C_m versus Alpha for Increasing Camber

As alpha changes, the c_m fluctuates as shown above. NACA 0012 has zero pitching moment when angle of attack, alpha, is zero because it acts as a symmetric airfoil. However, as NACA 4412 produces the most lift, at c_{l0}, it also has the largest moment coefficient.

Plots of c_d vs. alpha for five airfoils with increasing camber follow in Figure 5.3. The plots show how c_d increases with an increased alpha.
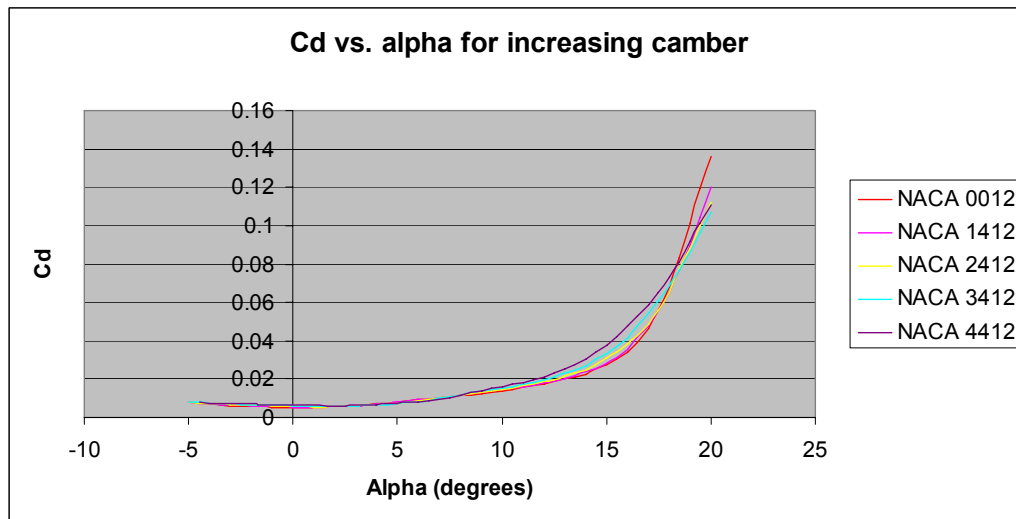
Figure 5.3 C_d versus Alpha for Increasing Camber

The coefficients of drag for the five airfoils are similar. This shows that an increase in camber does not greatly affect the drag produced by each airfoil.

Plots of drag polar c_d vs. c_l for five airfoils follow in Figure 5.4. The optimal point for cruise would be the point with the highest c_l/c_d which is the point furthest to the right for each plot.
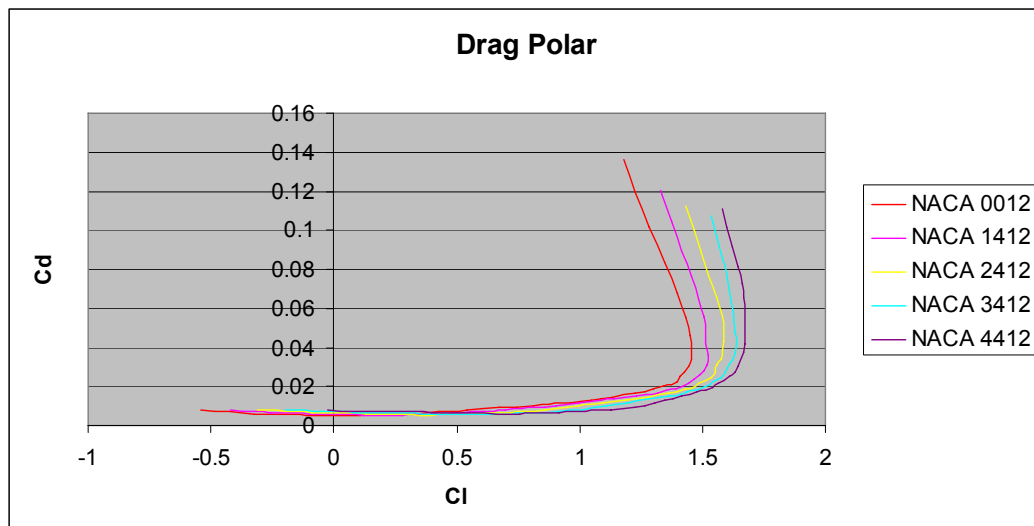
Figure 5.4 Drag Polar

Since the drags for the five airfoils are similar, the airfoil with the highest lift to drag ratio, L/D, would be the NACA 4412 airfoil.

Ultimately, the NACA 4412 airfoil was chosen for its high c_{l0} and c_{lmax}, a low drag, a small center of pressure movement across large speed range, a reasonable pitching moment.

5.2 Wing Sweep

Wing sweep serves the purpose of reducing transonic shock and supersonic flow. However, since the UAV's maximum speed is below Mach 0.2, wing sweep would not be required as it would add to manufacturing cost. [5.4] However, if the aerodynamic center of the aircraft needs to be moved back far enough for balance, swept wings may be an option.

5.3 Taper

Tapered wings are used to simulate an elliptical wing loading. An elliptical wing loading is desirable as it minimizes induced drag for a given span. Thus, a plot was generated on MATLAB from the following equations and assumptions to obtain a taper ratio for a minimum wing area. A taper ratio will save material and allow for a higher wing loading.

From lifting line theory, [5.5]:

Assumptions include: elliptical wing loading, size of planform does not affect the weight of the aircraft (weight is kept constant at gross takeoff weight), effect of the canard is small, and steady level flight.

Variables :

C_l=lift coefficient

$\Gamma(y)$ =vortex distribution

c(y)=chord length along planform

V=velocity

b=span

S=planform area

L=W=603 lb (from constrain analysis)

$$c_l = \frac{L'}{0.5\rho V_\infty^2 c(y)} = \frac{2\Gamma(y)}{V_\infty c(y)} = \frac{2\Gamma}{V_\infty c(y)}\sqrt{1-(2y/b)^2}\;_s \qquad\qquad 5.1$$

$$c(y) = c_s(1-\frac{|y|}{2b}) \rightarrow \alpha - \alpha_{lo} = \frac{\Gamma(y)}{2V_\infty b}\left[1+\frac{2\Gamma b\sqrt{1-(2y/b)^2}}{\pi c_s(1-|y|/b)}\right] \qquad 5.2$$

$$c_l = \frac{2\Gamma}{V_\infty c_s}\frac{\sqrt{1-(2y/b)^2}}{1-|y|/b} = \frac{2\Gamma_s}{V_\infty c_s}f(y) \qquad\qquad 5.3$$

For minimum wing area, f'(y)=0,taper ratio =0.5

y =b/4
f(y=b/4)=$(3/4)^{-.5}$

$$c_l = \frac{2\Gamma_s}{V_\infty c_s}f(y) => \frac{\Gamma_s}{c_s} = \frac{c_{l\,max}V_\infty}{2f(y)} \qquad\qquad 5.4$$

$$\Gamma_{max}b = 4/\pi \times \frac{L}{\rho V_\infty^2} \qquad\qquad 5.5$$

$$\frac{\Gamma_{max}b}{\Gamma_s/c_s} = bc_{max} \qquad\qquad 5.6$$

$$S_{min} = .75bc_{max} = 68\,ft^2 \qquad\qquad 5.7$$
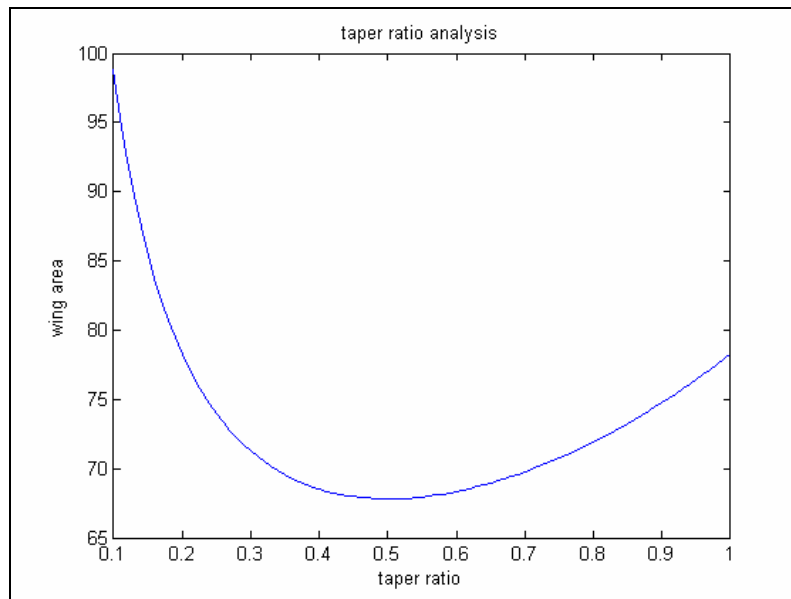
Figure 5.5 Wing Area versus Taper Ratio

When compared to a wing without taper ratio, a savings of over 10% of material results by using a taper ratio of 0.5 (minimum point on graph). Therefore, the wing area is reduced from 78 square feet to 69 square feet. From this wing area and an aspect ratio of 13 which was obtained from the constrain analysis, the resulting span (b) was 30 feet and the maximum chord length (cs) was 3 feet. The maximum lift coefficient (C_{lmax}) for the entire wing was also obtained as 1.45.

5.4 Twist

To obtain an elliptical wing loading, wing twist must be added. [5.5]

$$\delta = k - 1 \qquad\qquad 5.8$$

Where δ is twist and k is elliptical efficiency

Since the wing is tapered, the elliptical efficiency would be close to 1, about 1.04. [5.6]

Thus we'll yield a wing twist of 0.04 radians or 2.23 degrees.

Based on the taper ratio and wing twist, an elliptical wing loading can be obtained which in turn reduces induced drag.

6.0 Propulsion System

The propulsion system for the Metro-Scout is a pusher piston propeller engine as mentioned in section 3.3. To reiterate, it will be best located at the back of the airplane thus making it a pusher propeller type. This configuration is the best for the Metro-Scout because the camera part of the payload is in the nose. The propeller blades need to be out of the line of site of the camera. Placing the propulsion system in the front of the aircraft would not only obstruct the view of the camera but it would also create very turbulent flow around the camera creating extra vibrations and noise that will distort the picture.

6.1 Engine Selection

The initial horsepower requirement of the engine, 40 brake horsepower, was determined based on the weight, endurance, range, max speed, and power loading constraints of the UAV. This value was then taken to the UAV database to find off-the-shelf engines that met the power requirement. Table 6.1 shows the list of engines that were initially considered.

Engine	Lightening Aircraft Engines 604D4-F1	AR 801	AR 801R	Rotax 503	Rotax 582
Power (bhp)	50 +	35-60	51	45.6-49.6	53.6-65
RPM	6500	8000	8000	6800	6800
SFC		0.56	0.57		
Weight (lbs)	41	43	56		

Table 6.1: Engine List [6.1][6.3]

The AR-801 is a Wankel-type rotary, single rotor engine with a capacity of 294cc, brake horsepower of 35-60bhp at 8000RPM, and a specific fuel consumption of 0.56 at max power. It was chosen for its size, weight, specific fuel consumption and brake horsepower. The AR-801 engine has dimension of 1foot x 1.06 feet x 0.82 feet. This engine is known to be a highly optimized, light-weight, single rotor, liquid cooled engine. It is designed such that the mounting of alternators between 0.9 and 2.0 KW is feasible. It has been designed and developed specifically for UAVs requiring 35 to 60 bhp, with direct drive to propeller or vehicle gearbox. Other engines built by the same company are currently being used in other UAVs such as the RQ-6 Outsider and RQ-7 Shadow-200. [6.2] Below is a list of the major advantages to the use of this particular engine. Figure 6.1 is a picture of what the

AR-801 engine looks like with 4 blades. This is currently the chosen engine for the Metro-Scout.

Figure 6.1: AR-801 engine [6.1]

Use of an AR-801 engine: Advantages:

Team 4 has chosen the AR-801 UAV engine for the Metro-Scout for the following reasons:

(1) *High Power to Weight Ratio*: A larger power to weight ratio allows for better speed control and maneuverability of smaller aircraft. It also helps to decrease the overall weight of the aircraft but still producing enough power to meet the power requirement.

(2) *Economic Fuel Consumption:* An economic fuel consumption allows for the aircraft to fly farther per gallon of fuel used. This in turn can increase the endurance time and range of the aircraft, thus allowing for more continuous area coverage.

(3) *Low Levels of Vibration:* Vibration levels are extremely important when dealing with aircraft design. The lower the levels of vibration, the less stress acts on the aircraft. In the instance of the Metro-Scout, this means that although there is more stress on the tail section, overall there is less stress on the aircraft as a whole.

(4) *Low Cross Sectional Area:* The low cross sectional area of the AR-801 engine helps to decrease the amount of drag that is produced. On the Metro-Scout the engine is not streamlined into the fuselage, it is in fact, a separate entity that it attached to the back of the tail section. In most cases the pusher prop engine creates a large amount of drag, but the lower the cross sectional area of the engine, the less it sticks out around the fuselage, and less additional drag is created.

(5) Long Life: Although the lifespan of the engine is not a requirement, it is a definite advantage for the engine to have a longer lifespan so that it doesn't have to be replaced often. Replacing engines is extremely expensive and time consuming.

This engine type supports a variable pitch propeller. The variable pitch makes it possible for the pilot to change the blade angle of the propeller at will in order to obtain the best performance of the aircraft engine. At take-off the propeller is set at the low blade angle so that the engine can attain the max allowable power and rpm. Shortly after take-off the angle is increased slightly to prevent overspeeding of the engine and to obtain the best climb conditions of the engine rpm and aircraft speed. When the aircraft has reached cruise or loiter altitude, the propeller can be adjusted to a comparatively high pitch for low cruising rpm. This would allow for the Metro-Scout to be much more adaptable to flight conditions in the instance of a high speed chase. [6.4]

6.2 Propeller Sizing

Although the engine came with a known size of propeller blades, they were too long for the current design of the Metro-Scout. The blades would have struck the ground on take-off and so in order fix this problem, the propeller blades were sized using the following method.

Using the power required, many other parameters and specifications of the engine were calculated. The advance ratio and the activity factor are two very important parameters when understanding the blade design of the propulsion system. The advance ratio, found in equation 6.1, is just based on velocity, rotational speed and diameter of the blades.

$$J = V/nD \qquad\qquad (6.1)$$

The advance ratio, much like the wing angle of attack, is the related distance the aircraft moves with one turn of the propeller. The advance ratio for the Metro-Scout is 0.1875. The activity factor is a measure of the effect of blade width and width distribution on the propeller and is a measure of the propeller's ability to absorb power. Equation 6.2 is the equation of the activity factor per blade.

$$AF_{perblade} = \frac{10^5}{D^5} \int\limits_{0.15R}^{R} cr^3 dr \qquad (6.2)$$

The average activity factor for small, light aircraft is approximately 100. The activity factor for the blades on the Metro-Scout is 97.

Equation 6.4 below shows how the thrust required was obtained. The coefficient of thrust (c_T) was found using the propeller polar relation, shown in equation 6.3 and figure 6.2, between the power coefficient and thrust coefficient.

$$\frac{c_T}{J^2} = m\frac{c_P}{J^2} + b \qquad (6.3)$$
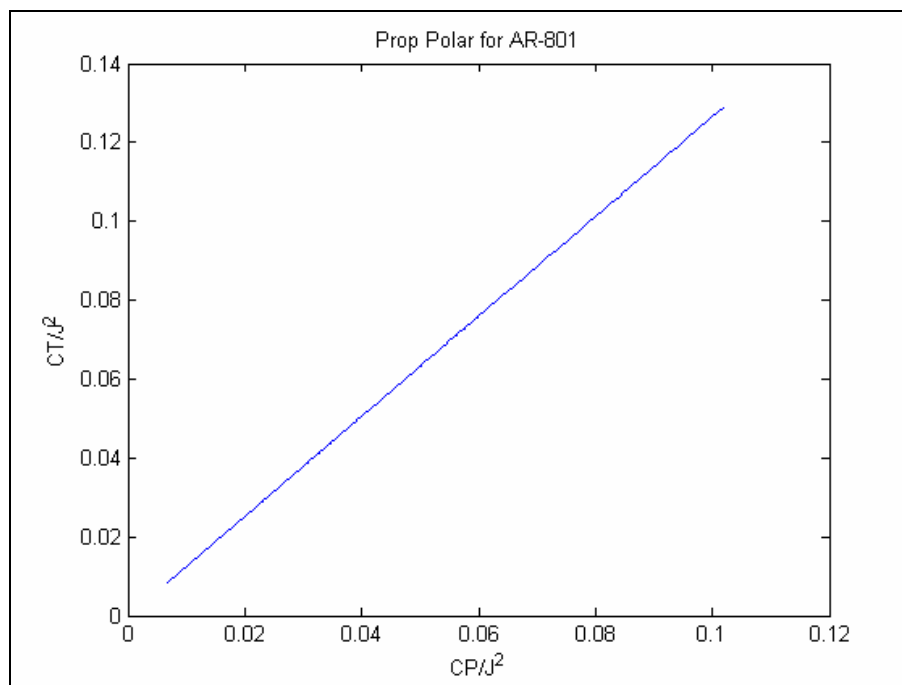
Figure 6.2: Propeller Polar Plot for AR-801 Engine

In equation 6.3, m and b are the slope and y-intercept of the propeller polar plot. The power coefficient (c_P) was found, seen in equation 6.4, since the power required was already known.

$$P = c_P \rho n^3 D^5 \qquad (6.4)$$

$$T = c_T \rho n^2 D^4 \qquad (6.5)$$

In equations 6.4 and 6.5, ρ is the density of air at sea level, n is the rotation speed, and D is the propeller diameter. From the thrust equation, equation 6.5, the propeller efficiency was calculated to be 0.76 in equation 6.6. [2.1]

$$\eta_P = \frac{TV}{550 * bhp} \qquad (6.6)$$

7.0 Longitudinal Stability Analysis

7.1 Stability Definition

The basic concept of stability is simply that a stable aircraft, when disturbed, tends to return, by itself, to its original state [2.1]. Stability is one of the important issues when building an aircraft. There are some terms associated with stability which are important to calculate and recalculate for optimization. These include center of gravity location (c.g), neutral point (n.p) and static margin (SM). Early estimations of what these values should be can help in determining the current stability of the aircraft. The methods of finding these variables are discussed here.

Before discussing the methods, some symbols and acronyms are to be noted:

M_{cg} -   moment about c.g

M_w -   wing aerodynamic pitching moment

M_c -   canard aerodynamic pitching moment

L_c -   canard lift

L_w -   wing lift

x_{ac_w} -   aerodynamic center of the wing (with respect to wing L.E)

x_{ac_c} -   aerodynamic center of the canard (with respect to wing L.E)

x_{cg} -   center of gravity location

α -   aircraft angle of attack

i_w -   wing incidence angle

i_c -   canard incidence angle

ε -   average downwash angle induced by canard

c_w -   wing mean chord

c_c -   canard mean chord

q -   dynamic pressure

S -   wing area

c -   aircraft chord length (fuselage length)

Figure 7.1 represents the free body diagram used as its base model. Taking into account all aspects of the force system, such as downwash and incidence angle, greatly complicates deriving an initial formula for neutral point. Thus, designers made several key assumptions in determining the initial analysis:

1) Drag and thrust are negligible

2) Downwash and fuselage effects are negligible

3) α is relatively small ($\cos(\alpha) \cong 1$)

4) $q_c = q_w = q$

5) Change in downwash angle with α is negligible ($\frac{\partial \varepsilon}{\partial \alpha} = 0$)

6) $\alpha_w = \alpha_c = \alpha$
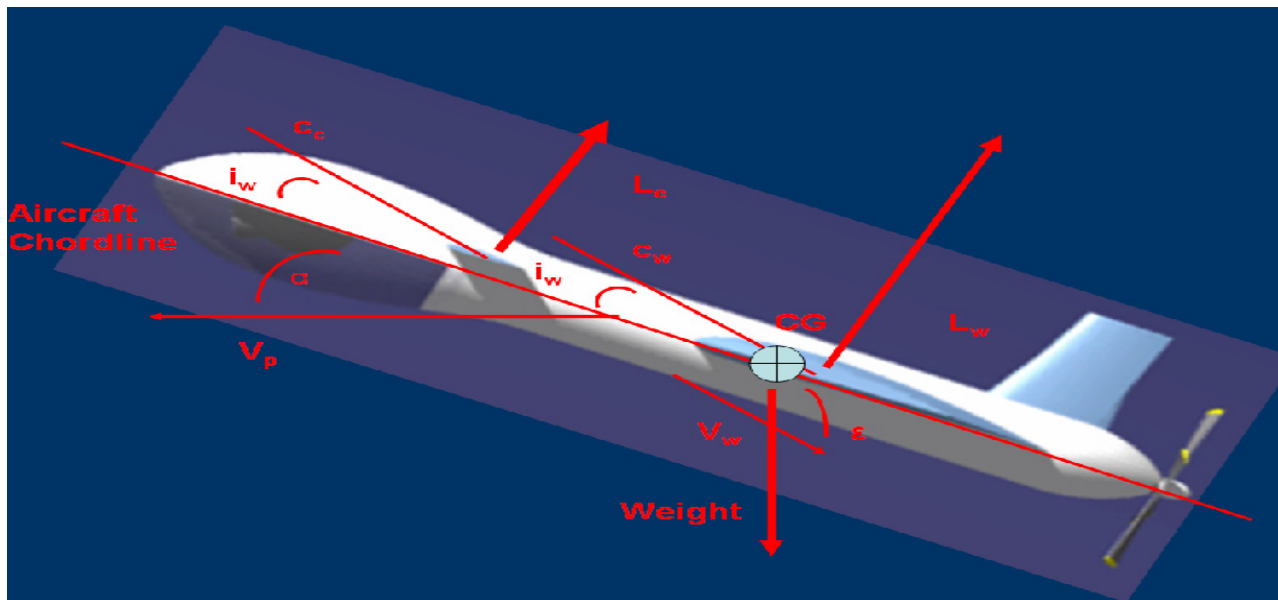
Figure 7.1 Free Body Diagram [7.1]

7.2 Neutral Point Calculation

The team set out to evaluate stability based on the location of the neutral point, or the point on the aircraft about which the net moment does not change with angle of attack [7.2]. This method essentially finds the point at which the aircraft center of gravity, c.g., rests in relation to the aircraft aerodynamic center. Figure 7.2 diagrams the forces on the aircraft and the locations of these forces with the designers' key assumptions in mind. Note that the reference location for this analysis rests at the leading edge of the wing.
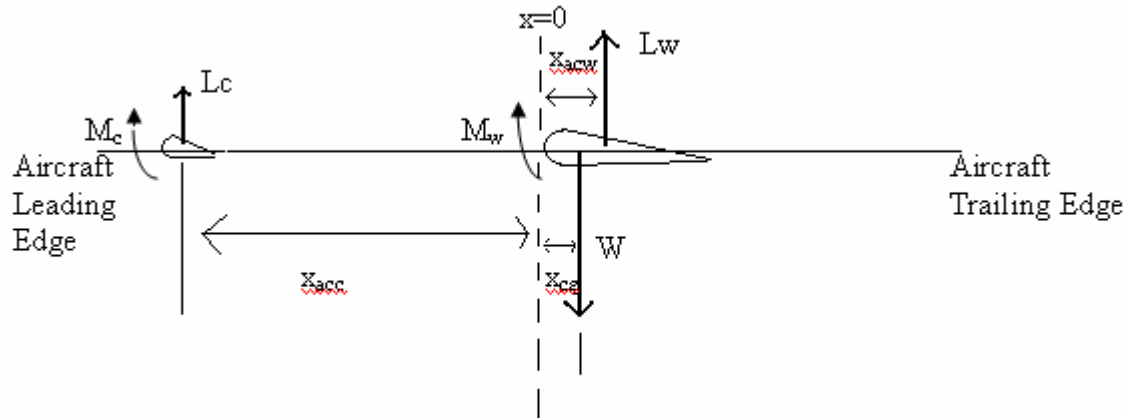
Figure 7.2: Forces and Reference Points for Neutral Point

Based on figure above, the team derived equation 7.1 for moment about the aircraft c.g..

$$M_{cg} = M_w - \left(x_{ac_w} - x_{cg}\right)L_w + M_c + \left(x_{cg} - x_{ac_c}\right)L_c \qquad 7.1$$

Originally, the equation looked like equation 7.2.

$$M_{cg} = M_w - \left(x_{ac_w} - x_{cg}\right)L_w \cos(\alpha + i_w - \varepsilon) + M_c + \left(x_{cg} - x_{ac_c}\right)L_c \cos(\alpha + i_c) \qquad 7.2$$

In equation 7.2, the group assumed α, i_w and ε were small (≈ 0) and thus the cosine term equals one, leading to Equation 7.1.

Next, designers altered equation 7.1 to create Equation 7.3 by dividing by aircraft mean chord, dynamic pressure, and wing area. This led to the non-dimensional coefficient form found in equation 7.4, where $c_m = M/qSc$ and $c_L = L/qSc$.

$$\frac{M_{cg}}{qSc} = \frac{M_w}{qSc}\frac{c_w}{c_w} - \frac{\left(x_{ac_w} - x_{cg}\right)}{c}\frac{L_w}{qS} + \frac{M_c}{qSc}\frac{c_c}{c_c}\frac{S_c}{S_c} + \frac{\left(x_{cg} - x_{ac_c}\right)}{c}\frac{L_c}{qS}\frac{S_c}{S_c} \qquad 7.3$$

$$c_{m,cg} = c_{m_w}\frac{c_w}{c} - \frac{\left(x_{ac_w} - x_{cg}\right)}{c}c_{L_w} + c_{m_c}\frac{c_c}{c}\frac{S_c}{S} + \frac{\left(x_{cg} - x_{ac_c}\right)}{c}c_{L_c}\frac{S_c}{S} \qquad 7.4$$

Analysis required multiplying each moment term in Equation 7.3 by the respective chord length of its component (c_w/c_w for the wing and c_c/c_c for the canard) to obtain the proper

moment coefficients for those components. Equation 7.5 represents Equation 7.4 after taking the derivative of each term with respect to its corresponding component's angle of attack.

$$c_{m,cg_\alpha} \alpha = c_{m,w\alpha}\, \alpha_w \frac{c_w}{c} - \frac{\left(x_{ac_w} - x_{cg}\right)}{c} c_{L,w\alpha}\alpha_w + c_{m,c\alpha}\frac{Sc}{S}\frac{c_c}{c}\alpha_c + \frac{\left(x_{cg} - x_{ac_c}\right)}{c}c_{L,c\alpha}\frac{S_c}{S}\alpha_c \quad 7.5$$

Again, the following terminology applies:

α_w – wing angle of attack

α_c – canard angle of attack.

However, $\alpha_w = \alpha_c = \alpha$ is one of the assumptions. Taking a derivative and setting equation 7.5 to be equal to zero yields equation 7.6.

$$c_{m,cg,\alpha} = 0 = c_{m,w\alpha} \frac{c_w}{c} - \frac{\left(x_{ac_w} - x_{cg}\right)}{c} c_{L,w\alpha} + c_{m,c\alpha}\frac{S_c}{S}\frac{c_c}{c} + \frac{\left(x_{cg} - x_{ac_c}\right)}{c}c_{L,c\alpha}\frac{S_c}{S} \quad\quad 7.6$$

The goal here is to find $\dfrac{x_{cg}}{c}$, hence rearranging equation 7.6 yields equation 7.7.

$$\frac{x_{cg}}{c} = \frac{\left(\dfrac{x_{ac_w}}{c}c_{L,w\alpha} - c_{m,w\alpha}\dfrac{c_w}{c} + \dfrac{x_{ac_c}}{c}c_{L,c\alpha}\dfrac{S_c}{S} - c_{m,c\alpha}\dfrac{c_c}{c}\dfrac{S_c}{S} \right)}{\left(c_{L,w\alpha} + c_{L,c\alpha}\dfrac{S_c}{S} \right)} \quad\quad 7.7$$

Finally, the team divided each term on the right hand side of equation 7.7 by $c_{L,w\alpha}$, and the **_final equation_** becomes equation 7.8.

$$\frac{x_{cg}}{c} = \frac{\left(\dfrac{x_{ac_w}}{c} - \dfrac{c_{m,w\alpha}}{c_{L,w\alpha}}\dfrac{c_w}{c} + \dfrac{x_{ac_c}}{c}\dfrac{c_{L,c\alpha}}{c_{L,w\alpha}}\dfrac{S_c}{S} - \dfrac{c_{m,c\alpha}}{c_{L,w\alpha}}\dfrac{c_c}{c}\dfrac{S_c}{S} \right)}{\left(1 + \dfrac{c_{L,c\alpha}}{c_{L,w\alpha}}\dfrac{S_c}{S} \right)} \quad\quad 7.8$$

As mentioned before, this $\dfrac{x_{cg}}{c}$ is actually the aircraft neutral point (n.p) ($\dfrac{x_{cg}}{c} = \bar{x}_{np}$) with respect to wing leading edge as the reference point. This implies that static margin is zero when $\bar{x}_{cg} = \bar{x}_{np}$ (here, $\bar{x}_{cg}$ is the actual c.g. location). Theoretically, c.g. can be forward

(ahead) or aft of the neutral point. To have a positive static margin which makes the aircraft stable, the c.g must be ahead of n.p based on the static margin formula in Equation 7.9.

$$SM = \bar{x}_{cg} - \bar{x}_{np} = \bar{x}_{cg} - \frac{x_{cg}}{c} \qquad 7.9$$

The variable $\bar{x}_{cg}$ is the actual c.g. location. By saying 'actual', this c.g. is derived from the following statistical group weight method.

The next step in determining the aircraft's stability involves determining the location of its center of gravity. The team used the statistical group weighted method summarized by equation 7.10 to accomplish this task.

$$\bar{x}_{cg} = \frac{\sum_{i=1}^{n} W_i \bar{x}_i}{\sum_{i=1}^{n} W_i} \qquad 7.10$$

Equation 7.10 sums the individual products of the weight of each main aircraft component (wings, canards, fuselage, etc.) at its respective center of mass and the component's distance from the leading edge of the aircraft. It then divides the result by the sum of the individual weights of the components. Figure 7.3 presents a visual model of this method. In a dynamical analysis, this method essentially treats each component as a particle mass located some distance from a reference point, which in this case, is the leading edge of the aircraft.
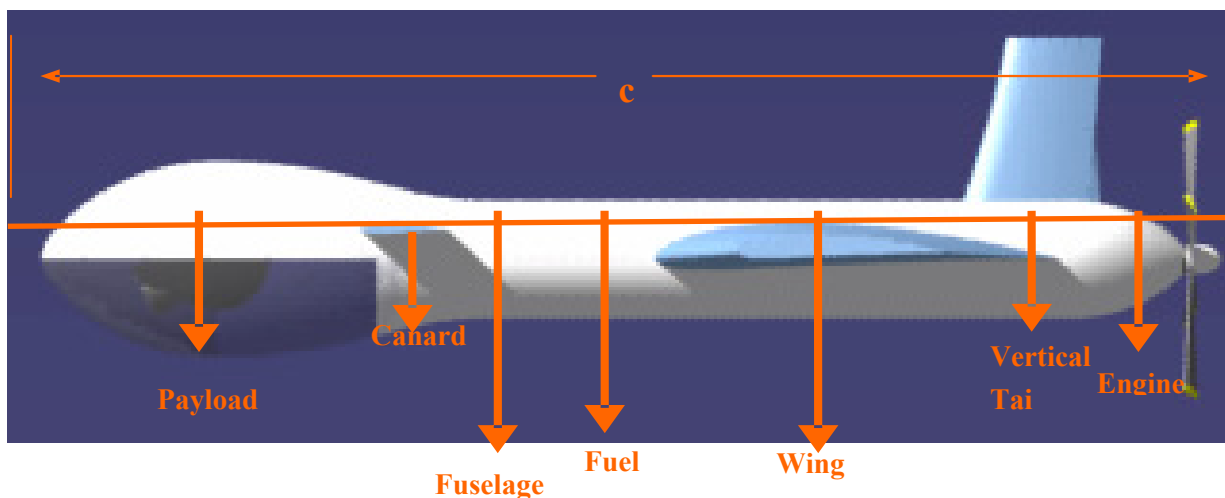
Figure 7.3: Geometry for Finding Aircraft Center of Gravity

Center of gravity depends upon fixed weights, such as those for the structure and payload, along with variable weights, such as that of fuel. Therefore, as the plane uses fuel during the flight, the center of gravity will shift, thus changing the static margin. For this reason, the team will place the tank containing a majority of the fuel as close to the center of gravity as possible to keep the center of gravity and, therefore, the static margin, from moving out of tolerance ranges during flight.

8.0 Summary

Thus far, Team 4 has determined to provide a primary customer base comprised of police and news organizations with the Metro-Scout, an unmanned aerial vehicle capable of performing those tasks for which those customers currently use conventional helicopters. This craft will perform both autonomously and with a remote pilot, depending on the mission such as safe operation at 1000-1500 ft above ground level, a coverage radius of 200mi, an endurance of at least five hours, and a payload weight of between sixty and seventy pounds. To perform such objectives, the team has determined key design attributes as outlined. The group aims to sell the Metro-Scout to target customers at a lower acquisition and operating cost than current helicopters to be competitive within the market.

After considering several possible designs for the aircraft, the team decided on a canard configuration with a front mounted camera and pusher piston propeller that would best accomplish the necessary missions. Airfoil selections as well as wing shape are currently in place to provide adequate lift, and the aircrafts longitudinal stability established by confirming the placements of both the center of gravity and the neutral point.

The next step forward in the design process involves several elements. First, the team must decide on an aspect ratio, which optimizes both aerodynamic need and structural limitations. There are also several aspects of the aircraft that will need additional optimization iterations in

order to create a better performance the required mission. The aircraft will need to be modeled, tested, re-evaluated, and eventually produced and distributed.

R.0 References

[1.1] "Bell Helicopter Commercial." 2007. Bell Helicopter Textron Inc. 28 Jan. 2007
www.bellhelicopter.com.

[1.2] AOPA, "AOPA's 2006 Aviation Fact Card",
download.aopa.org/epilot/2006/factcard.pdf [retrieved 18 February 2007].

[1.3] "The Helicopter Market Newsletter Piston", Helicopter International Association,
published Nov. 28th, 2005, http://www.rotor.com/market_letter/Piston_ML_Oct2005.pdf
[retrieved February 18th, 2007]

[1.4] "The Helicopter Market Newsletter Turbine", Helicopter International Association,
published Oct. 25th, 2005, http://www.rotor.com/market_letter/turbine_ML_Sept05.pdf
[retrieved February 18th, 2007]

[1.5] Clark, Larry K., "The Life of a Pilot Flying ENG (electronic news gathering),"
justhelicopters.com (online), 2/21/2004,
http://www.justhelicopters.com/Articles/detail.asp?iData=19&iCat=645&iChannel=2&nChannel=Articles , [retrieved February 15th, 2007]

[1.6] "2000 Aircraft Industry Studies", The Industrial College of Armed Forces,
http://www.ndu.edu/icaf/industry/2000/aircraft/aircraft4.htm , [retrieved Feb. 15th, 2007]

[2.1] Raymer, Daniel. P., *Aircraft Design: A Conceptual Approach* (4th Ed.), Blacksburg, VA:
AIAA Inc, (2006).

[2.2] Kroo, Ilan., Shevell, Richard., Chapter 12.1, Aircraft Design: Synthesis and Analysis ,
Retrieved April 1st, 2006, from http://adg.stanford.edu/aa241/noise/noise.html, ©
Desktop Aeronautics Inc., (2006).

[2.3] Lennon, Andy., *Canard: A Revolution in Flight (1st Ed.)*, Hummelstown, PA: Aviation
Publishers, (1984).

[3.1]Clausing, Don. Total Quality Development. New York: ASME P, 1994. 150-164.

[3.2] "Mobile police radar gun" simicon specifications page
http://www.simicon.com/eng/product/gun/radis.html [Retrieved 10-Feb-07].

[3.3] "Pixel 275 III" polytech specifications page
http://www.polytech.us/pixel275III_specs.htm [Retrieved 10-Feb-07].

[3.4] ThermaCAM® SC3000 Flir Systems therma cam specification page

http://www.flirthermography.com/media/SC3000%20datasheet.pdf

[Retrieved 10-Feb-07].

[3.5] Hal, "Sony Dvcam DSR-PD150 DV Specifications" product wiki database

http://www.productwiki.com/sony_dvcam_dsr_pd150_dv/article/sony_dvcam_dsr_pd150_dv_specifications.html [Retrieved 10-Feb-07].

[3.6] "3400 Full featured UAV autopilot" 3400 Auto pilot specifications

http://www.u-nav.com/3400autopilot.html [Retrieved 10-Feb-07].

[3.7] "Specification PowerShot S3 IS" S3 IS specifications

http://www.usa.canon.com/consumer/controller?act=ModelTechSpecsAct&fcategoryid=144&modelid=13077 [Retrieved 10-Feb-07].

[3.8] "Specifications EF 55-200mm f/4.5-5.6 II USM" EF f/4.5-5.6 II USM specifications

http://www.usa.canon.com/consumer/controller?act=ModelTechSpecsAct&fcategoryid=150&modelid=9435 [Retrieved 10-Feb-07].

[3.9] "C I N E F L E X V 1 4 M A G N U M - M U LT I S E N S O R" Cineflex 14 M Specifications

http://www.helinetaviation.com/downloads/pdf/Cineflex_Magnum_V14-MS.pdf

[Retrieved 10-Feb-07].

[5.1]Husa, B "Airfoil Selection" http://www.oriontechnologies.net/Documents/Airfoil.htm

[Retrieved April 2nd 2007]

[5.2] "NACA Airfoil Series" http://www.aerospaceweb.org/question/airfoils/q0041.shtml

[Retrieved April 2nd 2007]

[5.3]Heperlle, M "Location of Camber and Moment Coefficient"http://www.mh-aerotools.de/airfoils/nf_5.htm [Retrieved April 2nd 2007]

[5.4]Abbott, I.H., and von Doenhoff A. E., " Theory of Wing Sections: Including a Summary of Airfoil Data", Dover, pp 288.

[5.5]Lyrintzis, A.S., "AAE 514 Intermediate Aerodynamics Spring 2006", Copymat, West Lafayette, 2006,pp 59-62.

[5.6]"Induced drag", http://en.wikipedia.org/wiki/Induced_drag [Retrieved April 2nd 2007]

[6.1] "AR801 - 50bhp." UAV Engines Ltd. 2004. UAV Engines Ltd. 27 Feb. 2007

http://www.uavenginesltd.co.uk/index.php?id=402

[6.2] "Shadow-200." Unmanned Aerial System. 2005. AAI Corp. 25 Mar. 2007
http://www.aaicorp.com/New/UAS/html/shadowr_200.html

[6.3] "Rotax® 503UL DCDI." 1999. Kodiak Research Ltd. 6 Mar. 2007
http://www.kodiakbs.com/engines/503.htm

[6.4] Bent, Ralph D., and James L. McKinley. *Aircraft Powerplants*. 5th ed. NY, NY: McGraw-Hill Book Co., 1985. 375-383.

[7.1] Roskam, Jan. Airplane Flight Dynamics and Automatic Flight Controls. 4th ed. Lawrence, KS: DARcorporation, 2003.

[7.2] Steve, Brandt. Introduction to Aeronautics: a Design Perspective. Reston, VA: American Institute of Aeronautics, 2004.

A.0 APPENDIX

A.1 Project Timeline Description

Team 4 elected to develop a project timeline to establish a baseline measure of progress through the course of the semester. Team 4 has specifically targeting a number of phases in the design for overlap to allow the team greater freedom to make design changes and foster greater customer participation in formulating design requirements. For instance, the project timeline shows that Customer Attribute Identification phase goes hand in hand with the Initial Conceptual Design phase until the date of the Systems Requirements Review whereat all the customer attributes need to be finalized. The same is true for certain aspects of the Initial Conceptual Design and the Design Analysis and Tweaking phases. The premise behind the layout of the timeline is to establish constraints and deadlines that keep Team 4 moving forward in the design process while giving it the freedom to make changes as deemed necessary to keep the project competitive. The five main stages in Team 4's timeline and their current progress are –

(1.)	Establish Customer and Product:	Phase Complete
(2.)	Customer Attribute Identification:	Phase Complete
(3.)	Initial Conceptual Design	Phase Active
(4.)	Design Analysis/Tweaking	Phase Active
(5.)	Design Finalization	Planned/Not Active

		Task Name	Duration	Start	Finish
1	✓	⊟ Establish Customer & Product	8 days	Tue 1/16/07	Thu 1/25/07
2	✓	Identify Market Potential	5 days	Tue 1/16/07	Mon 1/22/07
3	✓	Identify & Differentiate Customers	8 days	Tue 1/16/07	Thu 1/25/07
4	✓	⊟ Customer Attribute Identification	20 days	Mon 1/22/07	Fri 2/16/07
5	✓	Establish Customer Wants	20 days	Mon 1/22/07	Fri 2/16/07
6	✓	Translate into Engineering Characteri:	20 days	Mon 1/22/07	Fri 2/16/07
7		⊟ Initial Conceptual Design	37 days?	Mon 1/22/07	Tue 3/13/07
8	✓	Establish Payload Configuration	19 days	Mon 1/22/07	Thu 2/15/07
9	✓	Choose Engine	18 days	Thu 2/1/07	Mon 2/26/07
10	✓	Sizing/Constraint Analysis	16 days?	Tue 2/20/07	Tue 3/13/07
11	✓	Choose Airfoil	12 days	Mon 2/19/07	Tue 3/6/07
12	✓	Tail Configuration	9 days	Mon 2/26/07	Thu 3/8/07
13	✓	Fuselage Configuration	14 days	Mon 2/19/07	Thu 3/8/07
14	▦	Design Pilot/Operator Command Stati	4 days	Thu 3/8/07	Tue 3/13/07
15	✓	Data Relay Set-up	4 days	Thu 3/8/07	Tue 3/13/07
16	▦	Landing Gear Set-up	6 days	Thu 3/1/07	Thu 3/8/07
17	▦	Safety Features - Decide and Design	19 days	Mon 2/12/07	Thu 3/8/07
18		⊟ Design Analysis and Tweaking	31 days?	Fri 3/2/07	Thu 4/12/07
19	▦	Aerodynamic Analysis	22 days?	Thu 3/8/07	Thu 4/5/07
20	▦	Propulsion Analysis	6 days?	Thu 3/8/07	Thu 3/15/07
21	▦	Performance Analysis	29 days?	Fri 3/2/07	Tue 4/10/07
22	▦	Safety Analysis	25 days	Thu 3/8/07	Tue 4/10/07
23	▦	Final Cost Estimates	9 days	Mon 4/2/07	Thu 4/12/07
24	▦	Mission Simulation	12 days?	Thu 3/22/07	Fri 4/6/07
25	▦	Final Tweaks	6 days?	Fri 3/30/07	Fri 4/6/07
26		Final Test	2 days?	Mon 4/9/07	Tue 4/10/07
27		⊟ Design Finalization	5 days	Fri 4/13/07	Thu 4/19/07
28	▦	Decision to Finalize all Aspects	3 days	Fri 4/13/07	Tue 4/17/07
29	▦	Report Write-up	5 days	Fri 4/13/07	Thu 4/19/07

Figure A.1: Gantt chart – Team 4's Project Timeline

A.2 UAV Database

Database sources:

www.shephard.co.uk/UVonline

www.fas.org/irp/program/collect/uav_roadmap

www.milnet.com/pentagon/uavs

http://csat.au.af.mil/2025/vol3ch13.pdf

http://uav.noaa.gov

www.navy.mil

UAV	Length (ft)	Wing Span (ft)	GW (lbs)	Payload (lbs)	Fuel Capacity (lbs)	Wf/W0	We/W0	Endurance(hr)	Power(hp)	Propulsion	Vmax (kts)	Vloiter (kts)	Ceiling (ft)
Predator	26.7	48.7	2250	450	665	0.295555556	0.504444444	24	115	piston prop	118	70	25000
Predator B	36	66	10500	750	4000	0.380952381	0.547619048	30	900 (shp)	piston prop	225		50000
Pioneer	14	17	452	75	76	0.168141593	0.665929204	5	26	piston prop	110	65	15000
Global Hawk A	44.4	116.2	26750	1950	14700	0.549532271	0.377570093	32	7800 (lbs)	turbofan	350	340	65000
Global Hawk B	47.6	130.9	32250	3000	16320	0.506046512	0.400930233	28	7800 (lbs)	turbofan	340	310	60000
Hunter A	22.6	29.2	1620	200	421	0.259876543	0.616666667	11.657 (x2)		piston prop	106	89	15000
Hunter B	23	34.25	1800	200	421	0.233888889	0.655	18.56 (x2)		piston prop	106	89	18000
Shadow A	11.2	12.8	327	60	51	0.155963303	0.660550459	5	38	piston prop	110	70	14000
Shadow B	11.2	14	375	60	73	0.194666667	0.645333333	7	38	piston prop	105	60	15000
X-45	39	49	36500	4500	14000	0.383561644	0.493150685	7		turbojet?	460		40000
X-47	38	62	46000	4500	17000	0.369565217	0.532608696	9		turbojet?	460		40000
I-GNAT	27	49	2300	450	625	0.27173913		30	115	piston prop	120	70	25000
Neptune	6	7	80	20	18	0.225	0.625	4	15	piston prop	84	60	8000
Prowler II	14	24	546	96			0.824175824	18		piston prop	125		20000
Altus	22	55	1200	330			0.725	24	100	turbo charged piston	125		18000
D'Humbug	6.5	6.5	180	25			0.555555556	4	36	piston prop	215		18000
Eagle Eye TR911B	18	13	2250	500			0.555555556	8		rotor	220		20000
Horus-SD	26.7	48.7	1042	450			0.665	40	105	piston prop	100		25000
KillerBee 4		10	172	66			0.581395349	16	450 V	electric	125	55	16000
Seascan II	4.6	9.5	45.6	19			0.592105263	80	82	piston prop	68	57	20000